

1 Carbon nanotube multilayered nanocomposites as multifunctional  
 2 substrates for actuating neuronal differentiation and functions of neural  
 3 stem cells

4  
 5 Han Shao <sup>1,3#</sup>, Tingting Li <sup>2,3#</sup>, Rong Zhu <sup>2,3#</sup>, Xiaoting Xu <sup>2,3</sup>, Jiandong Yu <sup>2,3</sup>,  
 6 Shengfeng Chen <sup>2,3</sup>, Li Song <sup>2,3</sup>, Seeram Ramakrishna <sup>2,3,4</sup>, Zhigang Lei<sup>5</sup>, Yiwen  
 7 Ruan <sup>2,3\*</sup>, Liumin He <sup>1,3\*</sup>

8 <sup>1</sup> Key Laboratory of Biomaterials of Guangdong Higher Education Institutes,  
 9 Department of Biomedical Engineering, College of Life Science and Technology,  
 10 Jinan University, Guangzhou 510632, China

11 <sup>2</sup> Guangdong-Hong Kong-Macau Institute of CNS Regeneration (GHMICR), Jinan  
 12 University, Guangzhou 510632, China

13 <sup>3</sup> MOE Joint International Research Laboratory of CNS Regeneration, Jinan  
 14 University, Guangzhou 510632, China

15 <sup>4</sup> Department of Mechanical Engineering, Faculty of Engineering, National University  
 16 of Singapore, Singapore 117576, Singapore

17 <sup>5</sup> Department of Anatomy and Cell Biology, Indiana University School of Medicine,  
 18 Indianapolis, Indiana 46202, USA.

19  
 20  
 21  
 22  
 23  
 24  
 25  
 26  
 27  
 28  
 29  
 30 # These authors contributed equally to this work.

31 Corresponding Author: Liumin He, Tel: 8620-8524338, E-mail: tlmhe@jnu.edu.cn.

32 Yiwen Ruan: tyiwen@jnu.edu.cn

**Abstract**

Carbon nanotubes (CNTs) have shown potential applications in neuroscience as growth substrates owing to their numerous unique properties. However, a key concern in the fabrication of homogeneous composites is the serious aggregation of CNTs during incorporation into the biomaterial matrix. Moreover, the regulation mechanism of CNT-based substrates on neural differentiation remains unclear. Here, a novel strategy was introduced for the construction of CNT nanocomposites via layer-by-layer assembly of negatively charged multi-walled CNTs and positively charged poly(dimethyldiallylammonium chloride). Results demonstrated that the CNT-multilayered nanocomposites provided a potent regulatory signal over neural stem cells (NSCs), including cell adhesion, viability, differentiation, neurite outgrowth, and electrophysiological maturation of NSC-derived neurons. Importantly, the dynamic molecular mechanisms in the NSC differentiation involved the integrin-mediated interactions between NSCs and CNT multilayers, thereby activating focal adhesion kinase, subsequently triggering downstream signaling events to regulate neuronal differentiation and synapse formation. This study provided insights for future applications of CNT-multilayered nanomaterials in neural fields as potent modulators of stem cell behavior.

**Key words:** Carbon nanotube multilayers, neural stem cells, differentiation, functions, molecular mechanisms

## Introduction

Since first discovered by Ijima in 1991, carbon nanotubes (CNTs) have attracted tremendous attention in biomedical applications as the forefront of nanotechnology owing to their unique structural, thermal, electrical, and mechanical properties<sup>1,2</sup>. CNTs can be classified into single-walled CNTs (SWCNTs) and multi-walled CNTs (MWCNTs). During the last decade, numerous studies have documented the outstanding performances of CNTs in neuroscience fields. Two application strategies are widely utilized. The first is the direct interactions of soluble CNTs with neural cells, where CNTs mainly serve as a nano-delivery system via cell uptake<sup>3-6</sup>. The second is the surface modification of supporting matrix for neural cell functions, where CNT-involved nanomaterials act as electrical interfaces of electrodes<sup>7-9</sup>, substrates for neural stem cell (NSC) growth and differentiation<sup>10,11</sup>, and scaffolds for axon growth in vivo<sup>12-15</sup>.

The size and shape of CNTs are similar to neuronal processes, which, combined with a large specific surface area and electric conduction, are the qualities advantageous for creating substrates for neural growth. Intracellular uptake of CNTs seldom occurs if the CNT-layered substrate is stable. Possible toxicity, thus, is less of a concern<sup>16</sup>. Accumulating data have demonstrated that the employment of CNTs provides a perspective platform for neurological research as promising substrates. CNT-layered substrates are biocompatible and efficient in inducing stem cells to differentiate specifically to neurons<sup>17-19</sup>, promoting neurite outgrowth<sup>20</sup>, and enhancing synaptogenesis<sup>21-23</sup> and consequential development of neuronal network<sup>24,25</sup>.

Modification of pristine CNTs is a prerequisite for biomedical applications due to their insolubility in organic and aqueous solvents. Oxidative treatment using concentrated strong acid (e.g., nitric and sulfuric acids) is the most utilized method. The carboxyl groups created in CNT caps and walls can be further utilized to react with the compound of interest via acylation, amidation, esterification, and PEGylation<sup>26</sup>. Chemical functionalization can also effectively purify CNTs and simultaneously improve the biocompatibility. However, oxidation unavoidably causes

defects to the nanotubes and consequently damages CNT bulk properties. Non-covalent modification became increasingly attractive in recent years and is achieved by coating or wrapping CNTs with polymers<sup>27</sup>, peptides<sup>28</sup>, proteins<sup>29</sup>, or single-stranded DNA<sup>30</sup> via  $\pi$ - $\pi$  stacking interactions<sup>31</sup>. Such non-covalent modification technology enables the preservation of CNT aromatic structure without harming their bulk properties. In a previous study, we modified MWCNTs via dopamine (DA) self-polymerization on the outer surface, which significantly improved MWCNT dispersibility in water<sup>16</sup>. Furthermore, the polydopamine-modified CNTs (CNT@PDA) can be utilized to fabricate multilayered nanocomposites with polyelectrocytes by using layer-by-layer (LbL) assembly. CNT-polymer composites are generally prepared by blending. Complete dispersion of CNT in a polymer matrix of high content, however, is rarely achieved until now despite the CNT modifications. Our study, therefore provided a common yet effective platform for the fabrication of CNT-based nanocomposites of high structural homogeneity with high CNT loading<sup>32,33</sup>.

NSCs are promising candidate seeding cells for the cellular repair of lesions of the central nervous system as they can primarily differentiate into neurons, astrocytes, and oligodendrocytes to replace the dead neural cells induced by injuries. Although studies are performed on the influences of CNT-based substrates on the behaviors of NSCs, the underlying mechanism is still not clearly understood. In this study, we presented a multilayered nanocomposite by alternating the LbL assembly of positively charged poly(dimethyldiallylammonium chloride) (PDDA) and negatively charged MWCNT prepared using DA self-polymerization<sup>16</sup>. The differentiation of NSCs and the growth and electrophysiological functions of NSC-derived neurons on the multilayered nanocomposites were thoroughly investigated. A high-throughput sequencing analysis of the whole transcriptome of the cultured cells was employed, and results provided a comprehensive picture of the potential molecular mechanisms underlying the interactions between these CNT-based nanobiomaterials and NSCs.

## Materials and Methods

## Materials

Pristine MWCNTs (>95% purity; OD: 10-20 nm; length: 0.5-2  $\mu$ m) and carboxyl-functionalized MWCNTs (named CNT-COOH herein) (>95% purity; OD: 10-20 nm; length: 0.5-2  $\mu$ m) were purchased from MK Impex Corp (Toronto, Canada). Dopamine (DA) and Tris-HCl from J&K Chemical (Shanghai, China), polyethyleneimine (PEI, Mn~60,000 Da) and poly(dimethyldiallylammonium chloride (PDPA, medium molecular weight) from Acros Organics (Geel, Belgium), and polylysine (PLL) from Sigma-Aldrich (St Louis, MO) were directly used without further treatment.

## Preparation of CNT-multilayered nanocomposites

CNT@PDA solution was prepared as described in a previous study<sup>16</sup>. In brief, 250 mg of pristine CNTs and 50 mg of dopamine hydrochloride were added into 500 mL of 10 mM Tris-HCl (pH = 8.5). The mixture was dispersed using ultrasonic treatment for 2 h followed by stirring for another 48 h at room temperature. A total of 100 mg of CNT-COOH was dissolved in 500 mL of ultrapure water by using sonication for 2 h to prepare the CNT-COOH solution. CNT@PDA and CNT-COOH collectively were called nanotubes hereafter unless specified.

Prior to the fabrication, quartz substrates were dipped into PEI solution for 30 min to obtain a positively charged surface. Then, the PEI-activated quartz substrates were immersed into the CNT@PDA suspension and PDPA solution (2.0 mg/mL in ultrapure water) for 20 min in turn. Each step was followed by washing three times with water. The cycle was repeated 10 times to obtain the CNT@PDA/PDPA multilayered films. The CNT-COOH/PDPA multilayered films were fabricated using the same methods.

## Characterization of CNT-multilayered nanocomposites

The buildup of the CNT@PDA/PDPA multilayered films and the CNT-COOH/PDPA multilayered films were measured using a UV-2505 spectrophotometer (Shimadzu, Kyoto, Japan). The morphology of the CNT multilayers was observed under a scanning electron microscope (SEM, JSM-TE300, JEOL, Japan) at an accelerating voltage of 20 kV after coating with gold by using a

sputter coater (JEOL JFC-1200 Fine Coater, JEOL, Tokyo, Japan). The topography of CNT multilayers was investigated by a Atomic force microscope (AFM, Bruker, USA) using Bioscope Catylyst Nanoscope-V operating in ScanAsyst mode. Height images were acquired using a silicon cantilever (Budget Sensors, Innovative Solutions Bulgaria Ltd.) with a nominal force constant of 5N/m and resonant frequency of 150 kHz. Water contact angles of the multilayered films were monitored using a contact angle measuring device (DKA100, Kruse, Hamburg, Germany).

### **Isolation and culture of mouse primary NSCs**

NSCs were isolated from the whole brain of embryonic day 14.5 (E14.5) female C57 mice (Guangdong Provincial Animal Center). In brief, pregnant mice were anesthetized with 1.25% tribromoethanol solution, and the whole brain was dissected and dissociated to single cells suspended in a DMDM/F12 (Gibco, USA) medium containing EGF (Gibco, USA), bFGF (Gibco, USA), penicillin-streptomycin (Gibco, USA), N2 supplement (Gibco, USA), GlutaMAX-I (Gibco, USA), heparin (MCE, HY-17567A), and B27 supplement. The cells were cultured, and after 2-3 days neurospheres formed, which were passaged approximately once per week. To confirm that the neurospheres were nestin-positive cells, the neurospheres were fixed with 4% formaldehyde in 0.1 M phosphate buffer solution (PBS, pH 7.4) for 30 min at room temperature. After rinsing in PBS, the neurospheres were labeled with monoclonal anti-nestin and incubated with fluorescent Alexa 568 donkey anti-mouse secondary antibody for 2 h at room temperature.

### **Cell viability assay**

After incubating NSCs on CNT multilayers for 24h, the samples were briefly washed with phosphate-buffered saline (PBS), and then CCK-8 reagent (Beyotime, China) was added into the wells at a ratio of 1:10 (CCK-8 medium) and cells were maintained at 37 °C for further 2h. After that, 100 µl aliquots were pipetted into a 96-well plate, and the absorbance at 450 nm for each well was measured in a microplate reader (Multiskan MK3, Thermo Scientific, USA).

### **Immunofluorescence assays**

NSCs of passage 2 (P2) were seeded onto four substrates at a concentration of

3.5 × 10<sup>4</sup> cells/cm<sup>2</sup>: quartz slice, PLL-coated quartz slice, CNT-COOH/PDDA multilayer-coated quartz slice, and CNT@PDA/PDDA multilayer-coated quartz slice. Single NSCs were cultured in a differentiation medium, namely, DMDM/F12 containing 2% B27 supplement (Gibco, USA), 1% penicillin-streptomycin, and 1% fetal calf serum (Gibco, USA). Fourteen days after cultivation, the NSCs were fixed with 4% formaldehyde in 0.1 M PBS (pH 7.4) for 30 min at room temperature. After incubation in 5% goat serum, 1% BSA, and 0.2% Triton X-100 in PBS for 2 h at 4 °C, the Neuronal Class III β-Tubulin (β III tubulin, Abcam, UK) and Glial Fibrillary Acidic Protein (GFAP, Abcam, UK), which are widely used to investigate the NSC differentiation, were utilized to specifically label neurons and astrocytes, respectively. The total numbers of neurons and glial cells quantified on each substrate after fixed have been counted, which were 1.7 ± 0.3 × 10<sup>4</sup> cells/cm<sup>2</sup>. Various immunofluorescent assays were performed to investigate the NSC growth and differentiation on the substrates, and the antibodies are presented in Table S1.

#### **Western blot**

Total proteins were extracted from the cells by using BCA reagent (Beyotime, China) to measure the concentration of proteins. A total of 15 μg of protein samples was separated on a 10% polyacrylamide gel and transferred onto polyvinylidene fluoride membranes (Millipore, USA). The membrane was blocked for 1 h with 5% defatted milk powder at room temperature and then incubated with synaptophysin (SY38, Abcam, UK), β III tubulin (Abcam, UK), GFAP (Millipore, USA), or GAPDH (Abcam, UK) primary antibody at 4 °C overnight. The blots were then washed three times with TBST and incubated with corresponding horseradish peroxidase-conjugated IgG secondary antibodies (Boster, USA) for 1 h at room temperature. The blots were developed in ECL chromogenic substrate (Millipore, USA) and the images were captured using a gel imager (UVITEC). The gray value of each band was measured by ImageJ (NIH, Bethesda, MD) software. The relative expression of each immunoreactive band was calculated by comparing the target protein band with GAPDH. There were 6 samples in each group for testing, and each sample was tested 3 times.



## Neuronal cytoskeleton 2D construction

The neurons differentiated from the NSCs on the material were labeled with  $\beta$  III tubulin, and the cytoskeleton of the neurons was constructed in two dimensions by using the Neurolucida software(11.09, MBF Bioscience, USA). The average length of the axons and dendrites of the neurons was quantitatively analyzed. We selected NSC-derived neurons with the longest neurite larger than 10  $\mu$ m which were defined as typical neurons. Neurites of 20 neurons on each substrate were randomly measured. 6 independent substrates were measured for each group.

## Electrophysiological investigation

Electrophysiological recordings were performed in whole-cell mode by using a MultiClamp 700B amplifier (Axon, USA). The bath solution contained 126 mM NaCl, 2.5 mM KCl, 2 mM  $MgCl_2$ , 2 mM  $CaCl_2$ , 1.25 mM  $NaH_2PO_4$ , and 10 mM D-glucose, at pH 7.4. The pipette solution for the whole-cell voltage-dependent current recordings and current-clamp experiments contained 125 mM KCl, 10 mM K-gluconate, 125 mM  $MgCl_2$ , 0.2 mM EGTA, 10 mM HEPES, 2 mM  $Mg_2ATP$ , and 0.5 mM  $Na_2GTP$ . The pH was adjusted to 7.25 with KOH, and osmolarity was at 270–290 mOsm/L. Membrane resting potentials were maintained in the range of -65 to -70 mV; step currents were injected at 5 mV/step to elicit action potentials (APs). 10 neurons on each substrate were randomly selected for electrophysiology measurements. 6 independent substrates were measured for each group.

## RNA sequencing (RNAseq) and analysis of differentially expressed genes (DEGs)

After the NSCs were cultured in the differentiation medium for 7 days on different substrates, total RNA was isolated using Trizol. The integrity was evaluated using Agilent 2200 TapeStation (Agilent Technologies, Santa Clara, CA). The RINe of each sample was above 7.0. In brief, mRNAs were isolated from the total RNA and fragmented to approximately 200 bp. Subsequently, the mRNAs were subjected to cDNA synthesis, adaptor ligation, and enrichment with a low cycle by using TruSeq RNA LT/HT Sample Prep Kit (Illumina). The purified library products were evaluated using Agilent 2200 TapeStation and Qubit 2.0 (Life Technologies) and then diluted to 10 pM for cluster generation in situ on HiSeq 2500 Paired-End Flow Cell



and subsequent sequencing (2 ×100 bp) on HiSeq 2500 Platform (Illumina). Raw reads were filtered by removing those with adapters or contaminations or those with more than 10% N bases and more than 20% bases whose quality assessment was <20. The clean reads were then aligned to the reference genome using the TopHat software, where each alignment had no more than two mismatches or two gaps.

The quantification of mRNA was counted by using GFOLD, then the RPKM value was calculated according to the following equation:

$$\text{RPKM} = \frac{\text{total exon reads}}{\text{mapped reads(millions)} \times \text{exon length(KB)}}$$

The gene expression level was calculated using the baseMean method, and DEGs were identified using the standard of more than two absolute fold changes and adjusted P-value <0.05. The differential expression equation was calculated by Audics equation according to Audics et al<sup>34</sup>.

To understand the functions of the DGEs, gene ontology (GO) functional enrichment and Kyoto Encyclopedia of Genes and Genomes (KEGG) pathway analysis were performed in the online server of Princeton GO term finder with the functional annotation of biological process provided (<http://go.princeton.edu/cgi-bin/GOTermFinder>) and (<http://www.genome.jp/>).

### Data analysis

All data were analyzed using the Statview 5.0 software. All data were shown as mean ± standard error. Results of the multiple experiment groups were compared using one-way ANOVA and Fisher's PLSD test. Statistical significance was considered at p< 0.05.

### Results and discussion

CNTs have recently attracted great interests as promising platforms for nerve regeneration as substrates due to their effectiveness in promoting neuronal differentiation, improving neurite growth, and modulating synaptic strength<sup>10,20,25,35</sup>.

The mechanisms underlying the stimulation of neuronal cell behaviors thus are absolutely important and should be fully understood. In the current study, CNT-multilayered nanocomposites were fabricated on quartz substrates by using LbL

assembly of negatively charged MWCNTs and positively charged PDDA according to previous studies<sup>16,32</sup>. Single cells (P2) were seeded on these substrates, and the cell behaviors were thoroughly investigated aiming for a comprehensive picture of the molecular mechanisms underlying the interactions between these CNT-based nanobiomaterials and NSCs (Fig. 1). Given that the CNT-multilayered nanocomposites were fabricated on the quartz substrates, the sterile quartz slices were defined as the control group in the experiments. The NSCs were also cultured on PLL-coated substrates, which provided a permissive environment for stem cell growth.

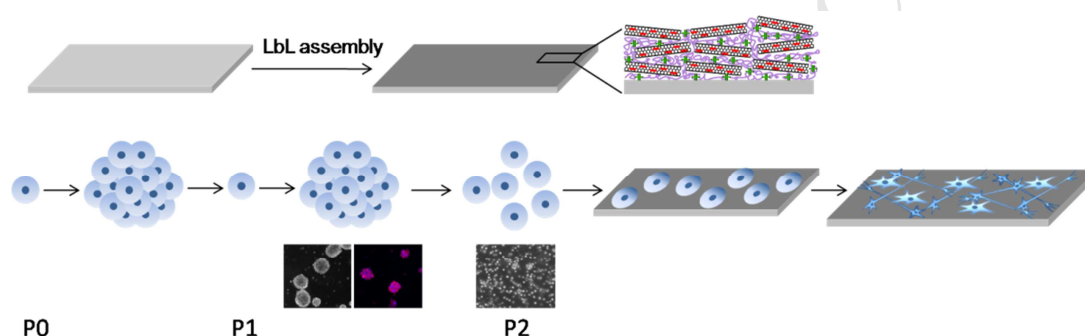


Fig. 1 Schematic diagram of the NSC differentiation on CNT-multilayered substrates. CNT multilayers were fabricated using the LbL assembly of negatively charged CNTs and positively charged PDDA according to previous studies<sup>16,32</sup>. After being passaged twice, E14.5 NSCs (P2) were cultured on the CNT-multilayered substrates in the differentiation medium.

DA can spontaneously self-polymerize under alkaline conditions into PDA, which strongly adheres onto virtually any type of solid surfaces<sup>36</sup>. In the current study, results of the morphological observation using TEM and analysis of the chemical structure using XPS jointly confirmed the successful PDA deposition on the surface of pristine CNTs<sup>16</sup>. Meanwhile, PDA deposition resulted in a negatively charged CNT@PDA surface, which was suitable for LbL electrostatic assembly with strong PDDA polycations. CNT-COOH was employed as a control. As both CNT@PDA and CNT-COOH showed strong UV absorbance at approximately 255 nm, the buildup process of CNT-multilayered nanomaterials was monitored using UV-vis spectrometry. The absorbance of the CNT@PDA/PDDA and CNT-COOH/PDDA multilayers both constantly increased with the assembly process, as shown in Fig. 2A and 2B. The absorbance intensity of these two CNT-based multilayers at approximately 255 nm

steadily increased in a nearly linear pattern with bilayer number, as indicated in the inset figures. One of the advantages of the LbL assembly technique is that it enables the preparation of films with any desirable thickness and architecture tailored to different applications. Flat surfaces were observed on the control and PLL-coating substrates (Fig. 2C and 2D). The final multilayers presented a mixture of individual CNTs and their bundles intricately interwoven together in a fine fabric, which uniformly covered the entire surface of the substrate without any evidence of phase separation (Fig. 2E and 2F). AFM was utilized to investigate the topography of CNT-COOH/PDDA (Fig. 2I) and CNT@PDA/PDDA (Fig. 2J) multilayers as compared with the control (Fig. 2G) and PLL-coating (Fig. 2H) substrates. The vertical properties were investigated by measuring the rootmean-square roughness (Fig. 4K). The CNT-COOH/PDDA and CNT@PDA/PDDA multilayers showed similar roughness, which were significantly higher than those of control and PLL-coating substrates. The CNT-COOH/PDDA and CNT@PDA/PDDA multilayer coating decreased the water contact angles compared with the quartz substrate as control (Fig. 2L). This result indicated of the good hydrophilicity of the CNT-based multilayers. Moreover, the smaller water contact angle of CNT@PDA/PDDA multilayers than that of CNT-COOH/PDDA multilayers was possibly attributed to the good solubility of PDA in water and its excellent coating of pristine CNTs.

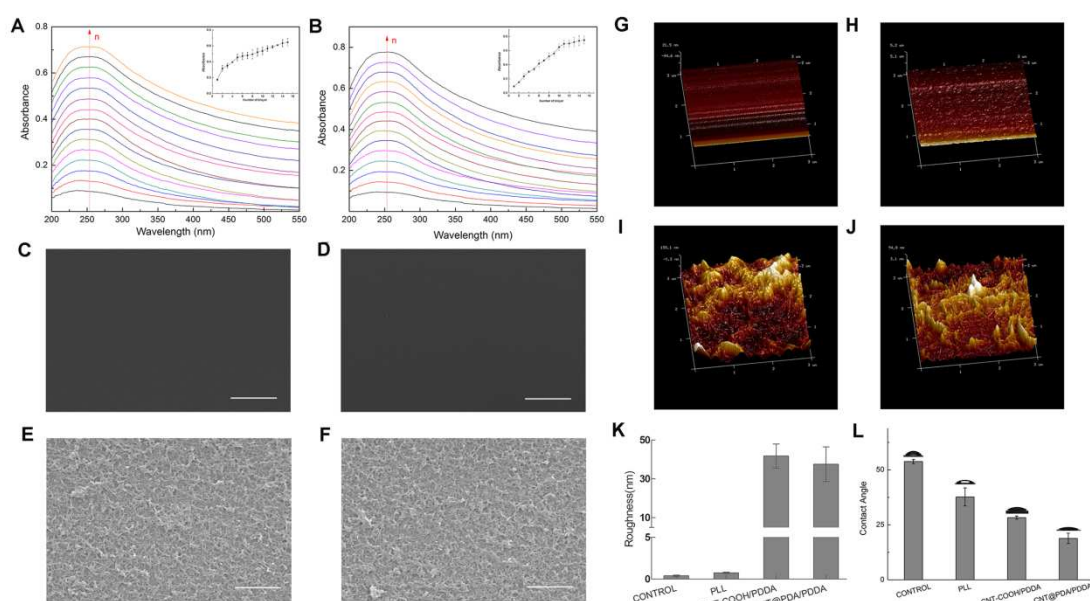


Fig. 2 LbL buildup of CNT multilayers with PDDA on a quartz slide. UV-vis absorption spectra and absorbance (inset) at 255 nm of the assembled (A) (CNT@PDA/PDDA)<sub>n</sub>-multilayered film and (B) (CNT-COOH/PDDA)<sub>n</sub>-multilayered film. SEM of (C) Control substrates, (D) PLL substrates, (E) (CNT@PDA/PDDA)<sub>15</sub> multilayers and (F) (CNT-COOH/PDDA)<sub>15</sub> multilayers. AFM of (G) Control substrates, (H) PLL substrates, (I) (CNT@PDA/PDDA)<sub>15</sub> multilayers and (J) (CNT-COOH/PDDA)<sub>15</sub> multilayers. The root-mean-squared roughness (K) and water contact angles (L) of various substrates. Scale bars: 2  $\mu$ m in C-F.

### Investigation of NSC differentiation on CNT multilayers

The neuron-specific cytoskeletal marker  $\beta$  III tubulin and GFAP were utilized to specifically label neurons and astrocytes 7 days after culturing NSCs under a differentiation condition. As shown in Fig. 3A, NSCs cultured on all substrates differentiated into neurons with long neurites and branches and into astrocytes with a multipolar glial morphology and long processes. Astrocytes with large multipolar and radially oriented morphologies dominated on the control substrate and PLL substrate. However, astrocytes on the CNT-COOH/PDDA and CNT@PDA/PDDA multilayers exhibited elongated somata and increased extension of processes. The typical morphology of a higher magnification is inserted at the top right corner of the figures. Astrocytic stellation/maturation is associated with a cell morphology that is further away from round<sup>37</sup>. Parpura et al. reported that water-soluble SWCNTs produce large and stellate/mature astrocytes when added to the culturing medium<sup>37</sup>. Therefore, the elongated astrocytic somata and increased extension of processes on the two CNT-multilayered substrates, especially on the CNT@PDA/PDDA multilayers, were consistent with morphological maturation. Similar results were also documented by Vicario-Abejón et al. NSC-differentiated astrocytes showed elongated morphologies on coverslips treated with thermally reduced graphene<sup>38</sup>. The differences in astrocyte morphology can be attributed to the nanoscopically rough surface of the CNT-containing substrates. More investigations are currently in progress in another study to further assess the modulation of the morphofunctional characteristics of astrocytes by CNT-multilayered nanomaterials.

The number of neurons and astrocytes was counted 7 days after the NSC differentiation on different substrates using the ImageJ software for quantization and

comparison (Fig. 3B and 3C). A total of  $42.1\% \pm 0.4\%$ ,  $37.3\% \pm 0.1\%$ ,  $27.4\% \pm 0.2\%$ , and  $32.8\% \pm 0.5\%$  tubulin+ cells were found on the CNT@PDA/PDDA multilayers, CNT-COOH/PDDA multilayers, control substrates, and PLL substrates, respectively. The percentage of GFAP+ cells was  $55.6\% \pm 0.05\%$  on the CNT@PDA/PDDA multilayers,  $51.5\% \pm 0.3\%$  on the CNT-COOH/PDDA multilayers,  $64.6\% \pm 0.3\%$  on the control substrate, and  $53.4\% \pm 0.6\%$  on the PLL substrate. These results showed that the CNT-multilayered substrates significantly enhanced the probability of NSC differentiation into neurons compared with smooth substrates without any exogenous differentiating factors. In addition, cell viability was measured using CCK8 assay due to its advantage in assessing the cytocompatibility of CNT-based materials<sup>39,40</sup>. As shown in Fig. 3D, the highest cell viability was achieved on the PLL substrate, followed by the CNT@PDA/PDDA multilayers, CNT-COOH/PDDA multilayers, and control substrate in a descending sequence. The differences between each substrate were statistically significant ( $n = 3$ ,  $p < 0.05$ ). Interestingly, cell viability showed a similar variation tendency on the substrates to astrocyte percentage (Fig. 3C). This finding indicated that the differentiated astrocytes mainly contributed to cell viability on the two smooth substrates. Our result was in good agreement with that of Kotov et al. when they studied the differentiation of mouse NSCs on LbL-assembled SWCNT-polyelectrolyte composites. In their study, a higher percentage of neuron differentiation and lower astrocyte differentiation were obtained on the SWCNT-multilayered films than those on poly-L-ornithine<sup>18</sup>. Therefore, CNT-based substrates provide a particularly more favorable environment for neuron growth than astrocytes.



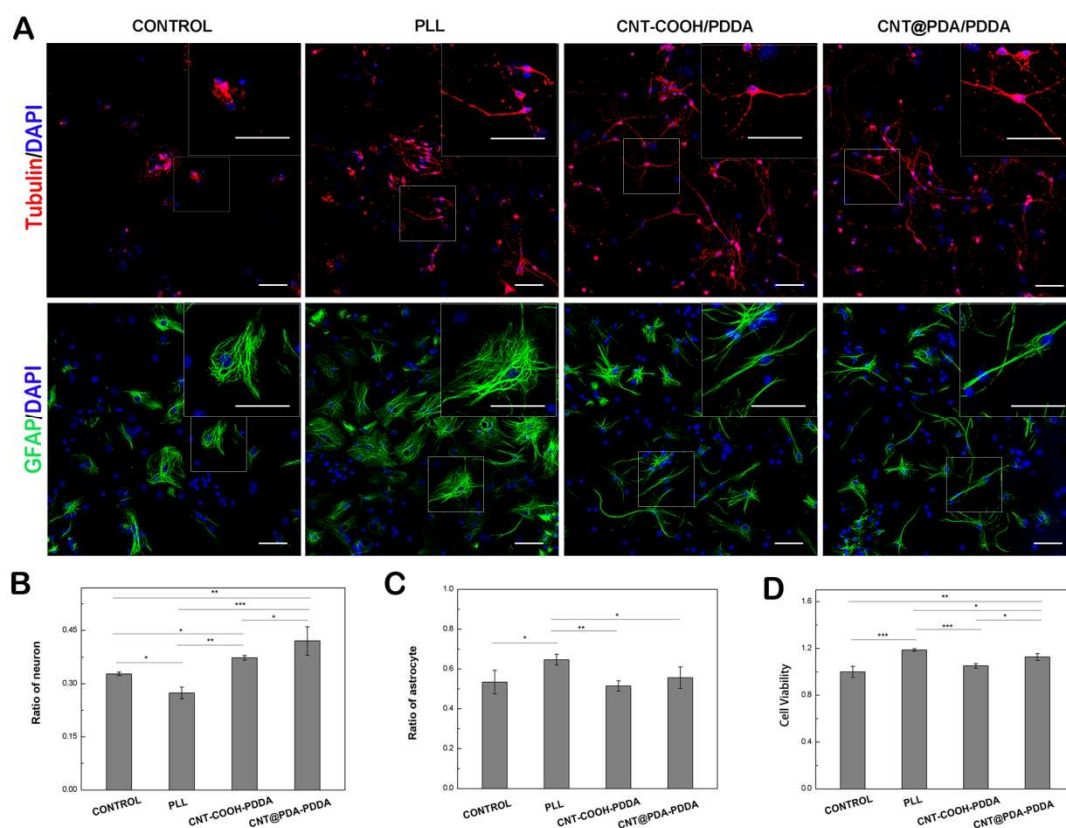


Fig. 3 NSC differentiation on various substrates in vitro. (A) Immunohistochemical staining of neurons (red,  $\beta$  III tubulin) and astrocytes (green, GFAP). Cell nuclei were stained using DAPI. The differentiation proportion of neurons (B) and astrocytes (C) and viability of NSCs on different substrates (D) were statistically analyzed.  $n = 3$  experiments,  $*p < 0.05$ . Scale bars: 50  $\mu$ m.

To determine whether the neurons differentiated from NSCs on the substrates could develop synapses, double immunostaining for synaptophysin (SY38) and neurons (MAP2) was performed. As shown in Fig. 4A, a punctuate staining pattern distributed around the MAP2<sup>+</sup> neuronal somata and extended along the entire network of neuronal processes on all substrates; this finding suggested the synaptic development and maturity of NSC-derived neurons. More synaptic vesicles were detected throughout the neuronal network on the CNT-multilayered substrates, especially the CNT@PDA multilayers, than on the smooth substrates (control and PLL substrates). Western blot analysis was further performed to investigate the effects of the CNT-multilayered nanocomposites on the differentiation of NSCs in vitro by using GAPDH as the calibrator protein. The expression levels of SY38 on the CNT-COOH/PDDA and CNT@PDA/PDDA multilayers were higher than those on

the control and PLL substrates. The expression levels of  $\beta$  III tubulin protein increased in the sequence of control, PLL, CNT-COOH/PDDA, and CNT@PDA/PDDA. The expression levels of GFAP protein, however, showed an inverse tendency on these substrates and decreased in the sequence of control, PLL, CNT-COOH/PDDA, and CNT@PDA/PDDA. Therefore, the results of molecular biology investigation further indicated that the CNT-multilayered nanocomposites demonstrated a preference for neuronal differentiation. A higher level of  $\beta$  III tubulin protein was expressed on the CNT@PDA/PDDA multilayers than on the CNT-COOH/PDDA multilayers although the difference was not significant. Hence, CNT@PDA was more advantageous than CNT-COOH. In sum, the CNT-multilayered nanocomposites provided matrices that were effective for stimulating NSC differentiation into neurons and synapse formation. This result was consistent with the aforementioned statistical analysis on NSC differentiation. The findings in the current agreed well with the results of previous studies on the promotion of NSC neuronal differentiation of CNT-based nanomaterials<sup>25,41</sup>. Moreover, the significantly higher level of SY38 protein on the CNT@PDA/PDDA multilayers than that on the CNT-COOH/PDDA multilayers ( $p < 0.05$ ) again indicated the advantages of PDA modification to CNT over the oxidative treatment.



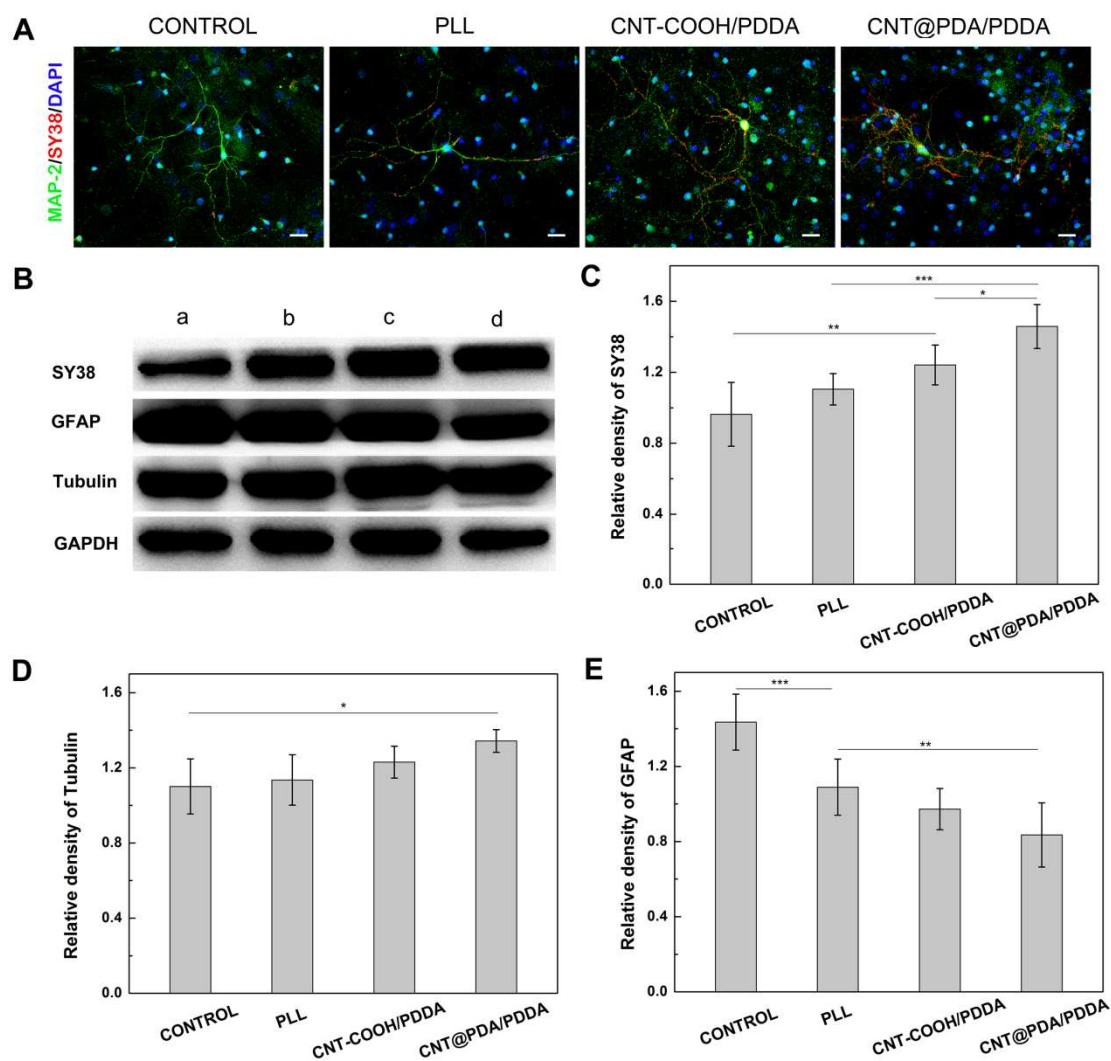


Fig. 4 Immunohistochemical staining of synaptic structures (red, SY38, co-staining with neurons in green, anti-MAP2) (A) and Western blot analysis of NSC differentiation on different substrates. (B) Agarose gel electrophoresis of  $\beta$  III tubulin, GFAP, and SY38. (C) Quantified protein levels of SY38-GAPDH, (D) tubulin-GAPDH, and (E) GFAP-GAPDH by using ImageJ (n=6). \* $p < 0.05$  and \*\* $p < 0.01$ . Scale bars: 20  $\mu$ m.

## Neurite outgrowth on CNT-multilayered nanocomposites

The morphological features of the differentiated neurons on the CNT-multilayered nanocomposites were thoroughly studied by characterizing the neurite outgrowth, including neurite length and branching. As shown in Fig. 5A, the neurons examined on control (n = 30), PLL (n = 33), CNT-COOH/PDDA (n = 79), and CNT@PDA/PDDA (n = 69) presented bipolar and multipolar characteristics with long neurites after 7 days. More branches and longer neurites were generally visualized on the CNT-multilayered substrates than those on the control and PLL

substrates. To quantify the neurite length and branching, a neuron cytoskeleton was reconstructed using the Neurolucida software (Fig. 5B). CNT@PDA/PDDA presented the longest total neurite per neuron and single longest neurite per neuron among the substrates investigated, followed by CNT-COOH/PDDA, PLL, and control in a descending sequence. Notably, the promotion of neurite extension on the CNT-multilayered substrates was more significant than on the PLL substrate, a well-known permissive substrate widely used as positive control for neuronal growth. Significant differences were found when CNT@PDA/PDDA with CNT-COOH/PDDA were compared; hence, CNT@PDA was advantageous in promoting neurite growth. Next, the neurite branching of the NSC-differentiated neurons on the CNT-multilayered nanocomposites was investigated. Neurite branching is an important determinant of established intercellular contacts and is vital to synaptogenesis and signal transduction. Substrate qualities play a role in the process of neurite branching<sup>42,43</sup>. Previous studies indicated that chemical functionalization enhances the branch formation of neurites compared with unmodified CNTs as substrates<sup>23,43</sup>. In the current study, the numbers of neurite and branches per neuron on the CNT-multilayered substrates were both significantly higher than those on the flat substrates ( $p < 0.01$ ), in a descending order of CNT@PDA/PDDA > CNT-COOH/PDDA > PLL > control. The results of neurite branching exhibited a similar pattern to that of neurite length. Neurites function as antennae of neurons, and their arborization is required for proper neuronal circuitry. Therefore, the CNT-multilayered nanocomposites fabricated in this study provided a permissive microenvironment for neurite outgrowth and also promoted the formation of new processes that increased the complexity of neuronal cytoarchitectures. Moreover, the CNT-multilayered nanocomposites promoted neuronal maturation, as characterized by an increase in neurite elongation and numerous branches<sup>44</sup>.

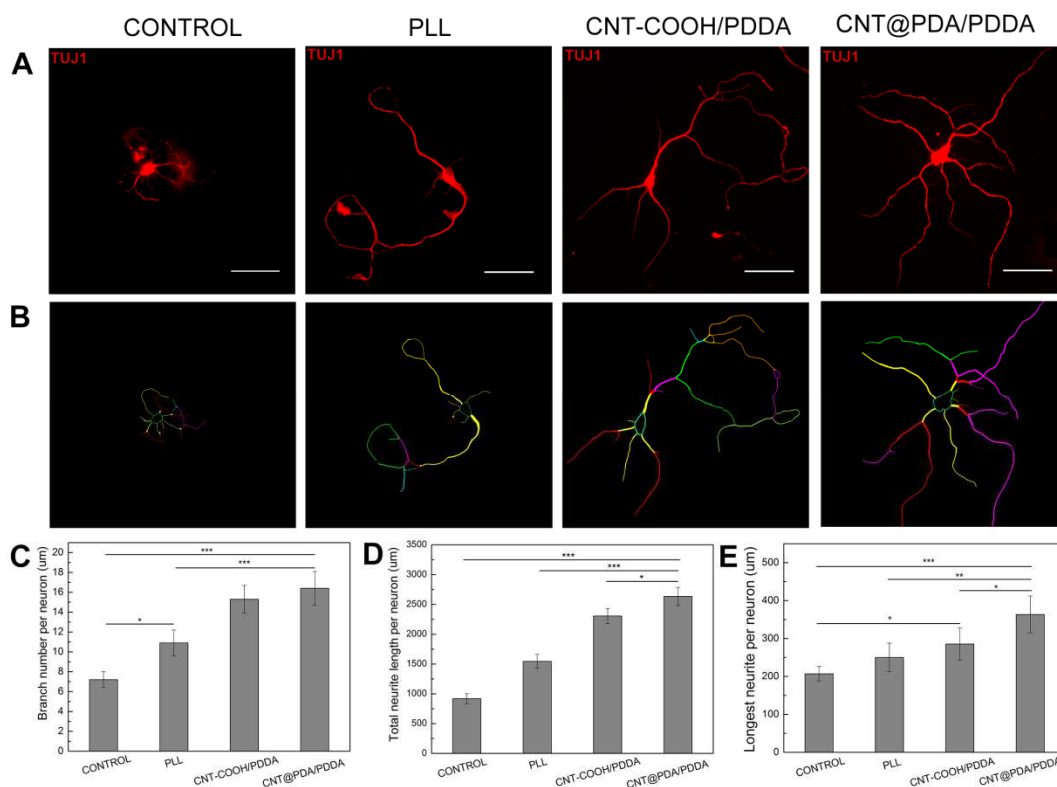


Fig. 5 2D reconstruction of neuronal cytoskeleton and quantitative analysis of neurite outgrowth. (A) NSC-derived neuron cultured on different substrates. (B) The contours of 2D structures of the corresponding neurons presented in (A). The number of neurites per neuron (C), total neurite length (D), and maximal length of neurite per neuron (E) were measured and quantitatively analyzed on various substrates. \* $p < 0.05$  and \*\* $p < 0.01$ . Scale bars: 50  $\mu\text{m}$ . (n=120)

GAP-43 and F-actin immunochemistry staining were performed together with  $\beta$  III tubulin labeling on the NSC-derived neurons to investigate the interactions between the neurites and substrates (Fig. 6). GAP-43 is a nervous-tissue-specific protein and is expressed in neurites, lamellipodia, and filopodia, where it associates tightly with the cortical membrane skeleton<sup>45</sup>. As shown in Fig. 6B1 and 6C1, GAP-43 was distributed at high levels along the neurites and was also weak to moderately present at the leading edges of the growth cone (arrowheads) on the control substrate. Immunoreactive lamellipodia and filopodia extending from the neurite were observed but were relatively small and short (arrows). By contrast, abundant immunoreactive lamellipodia and filopodia (arrows) along the long neurites and fan-like filopodia on the growth cone (arrowheads) were significantly observed on the PLL substrates (Fig. 6B2 and 6C2). Similarly, strong GAP-43 immunoreactive filopodia and lamellipodia were observed along the entire length and within the significant growth cones of the

neurites on the CNT-multilayered substrates (Fig. 6B3, 6C3, 6B4, and 6C4). F-actin was localized and distributed along the neurites and within the growth cones (arrowheads) as indicated by immunostaining for cytoskeleton with phalloidin, which was quite similar to GAP-43. The NSC-derived neurons on the CNT-multilayered substrates showed a similar expression within the growth cones to those on the PLL substrate. More F-actin immunoreactive filopodia and lamellipodia were even observed on the CNT-multilayered substrates than those on the PLL substrate. SEM was further utilized to visualize the interactions of the cytoskeletal processes of the NSC-derived neurons with the substrates. Short filopodia and lamellipodia were detected to extend from the neurites on the control substrate (Fig. 6G1), whereas abundant and long filopodia and lamellipodia were observed on the PLL substrate (Fig. 6G2). Moreover, a connection between cells at the neurite terminals was observed (arrowhead in Fig. 6G2). The neurites of the NSC-derived neurons on the CNT-multilayered substrates were well incorporated with the CNT-derived substrates. The growth fronts interacted intimately with the underlying CNTs with the filopodia and lamellipodia hardly identified (Fig. 6G3 and 6G4).

During development, neuronal growth cones play a major role in guiding the growing neurites to appropriate locations for the establishment of the correctly interconnected nervous system. Growth cones are composed of lamellipodia, from which thin filopodia with a submicron diameter emerge<sup>46</sup>. By gathering spatial, topographical, and chemical information with filopodia and lamellipodia, growth cones can sense nanotopographic features of the surrounding environment under the control of regulated actin polymerization<sup>44</sup>, which conversely affect integrin-mediated focal adhesion by reorganization of the cell cytoskeleton<sup>47</sup>. Abundant filopodia and lamellipodia structures within the growth cones and along the neurites during NSC differentiation on the CNT-multilayered substrates facilitated the growth of the growth cones and the development of focal adhesions. These results implied that NSC-derived neurons possibly possessed high affinity for the CNT-based nanomaterials. This behavior was understandable because the diameters of CNTs utilized in this study were tens of nanometers, similar to those of filopodia and

504 lamellipodia structures. These results agreed well with those by Gabay et al. and  
 505 Sorkin et al., in which cases neurons bound extremely well to CNT surfaces but not  
 506 adhere to the remaining spaces (free from nanotubes)<sup>48-50</sup>.

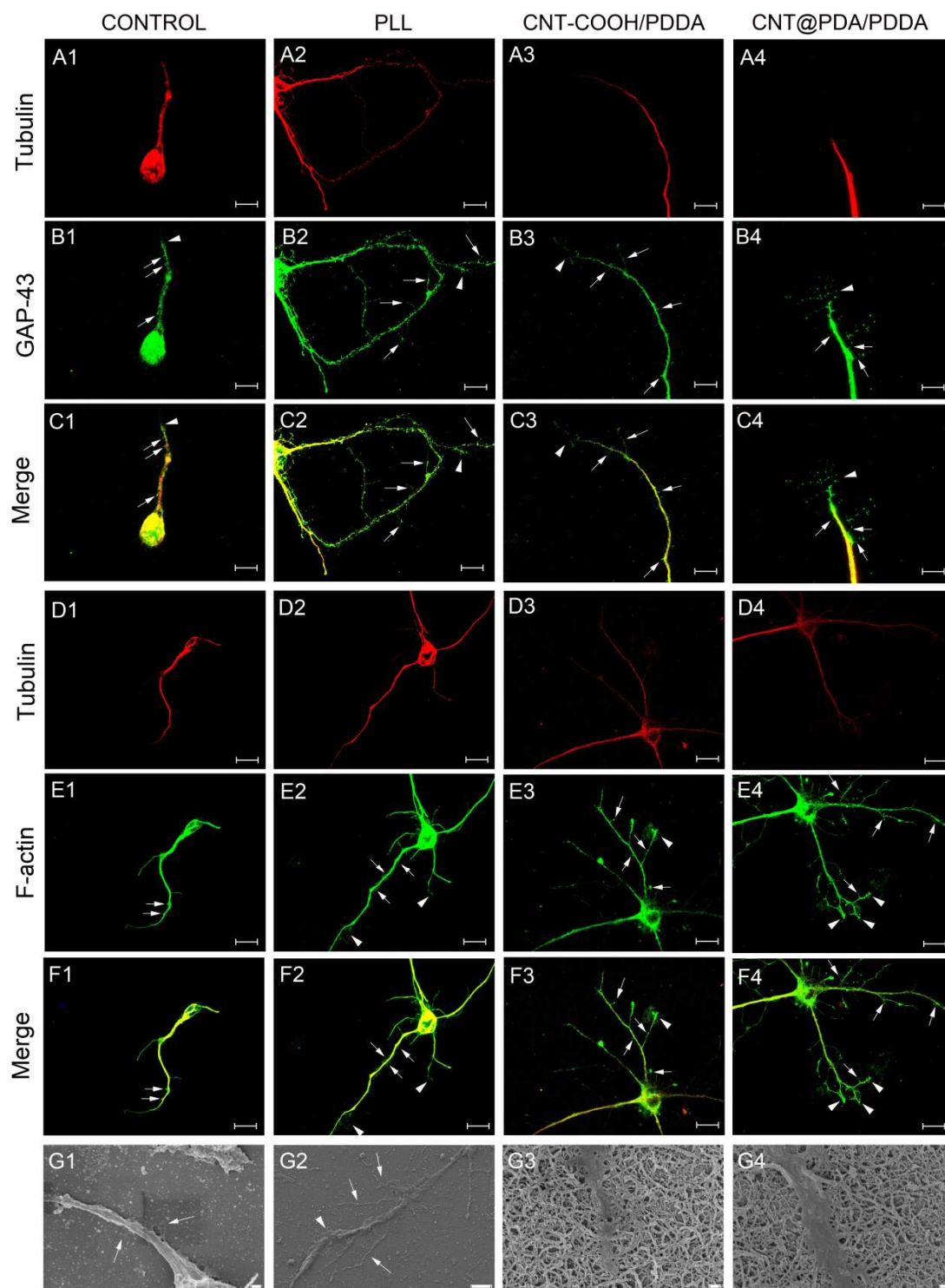


Fig. 6 Growth cone observation of NSC-derived neurons on different substrates. (A1-C4) GAP-43 and tubulin immunoreactive neurites. (D1-F4) F-actin and tubulin immunoreactive neurites. (G1-G4) SEM micrographs of neurites of NSC-derived neurons on different substrates. Lamellipodia and filopodia structures were present within the growth cones (arrowheads) and



along the neurites (arrows). Scale bars: 10  $\mu\text{m}$  in A1-F4; 200 nm in G1, G2, and G4; and 1  $\mu\text{m}$  in G2.

### **Electrophysiological function of NSC-differentiated neurons**

Neurons are electrically excitable cells that normally process and transmit information through electrical signals. Numerous studies indicated that neuronal electrophysiological functions can be affected by neuron-surface interactions. Neurons grown on a conductive substrate always display efficient signal transmission<sup>12,25,51</sup>. Most of the previous studies focused on adult neurons in vitro. Investigations on neurons differentiated from NSCs, however, were seldom reported. Here, we investigated whether the NSC-derived neurons on the CNT-multilayered nanomaterials exhibited electrophysiological functions. Whole-cell patch-clamp recordings were employed to test the basic electrophysiological properties of these NSC-derived neurons, such as the ability to fire APs and the induction of membrane current. Electrical stimulation from the holding potential of -70 mV, the resting membrane potential (RMP) of a typical neuron, at a 10 mV hyperpolarizing step was applied to the patched neurons. Passive and active membrane properties were quantified to evaluate the electrophysiological maturity and the variability of the NSC-derived neurons on the different substrates. In neurons, APs play a central role in cell-to-cell communication by providing for the propagation of signals at synapses. The representative trace of repetitive APs of the NSC-derived neurons on the different substrates is presented in Fig. 7A-7D. Mature AP spikes in response to depolarizing current injections were observed on all substrates, as confirmed by reaching a membrane potential above 0 mV with a fast depolarization and rapid repolarization<sup>52</sup>. A total of 12.5% (5/40), 20% (8/40), and 25% (10/40), 27.5% (11/40) of the recorded neurons fired mature APs on the control, PLL, CNT-COOH/PDDA multilayers, and CNT@PDA/PDDA multilayers, respectively. Among these mature AP-recorded neurons on CNT@PDA/PDDA, 36.4% (4/11) exhibited repetitive firing of mature APs. The remaining 63.6% (7/11) of neurons fired an initial mature AP followed by a sequence of APs that exhibited rapid accommodation (broad peaks other than spikes)

and no longer met the criteria for AP maturity. The percentages of recorded neurons that exhibited repetitive mature APs were 0% (0/5), 37.5% (3/8), and 40% (4/10) on the control, PLL, and CNT-COOH/PDDA multilayers, respectively. The number of mature AP spikes was counted on each depolarizing step and is presented in Fig. 7E. Mature AP-recorded neurons grown on the PLL substrate displayed the most spikes, followed by the neurons grown on the CNT@PDA/PDDA multilayers, CNT-COOH/PDDA multilayers, and control substrate. Neurons grown on the CNT@PDA/PDDA multilayers exhibited the lowest AP threshold (Fig. 7F), the minimum voltage needed for AP generation, and the highest AP peak among the neurons on the substrates in this study (Fig. 7G).

Neurons on the CNT@PDA/PDDA multilayers exhibited a RMP of  $-50 \pm 4$  mV, significantly lower than that on PLL substrate (Fig. 7H,  $p < 0.05$ ). Meanwhile, the RMP on the CNT-COOH/PDDA multilayers was also smaller than that on the PLL substrate despite no significant differences. The NSC-derived neurons possessed comparable membrane input resistances on all substrates of 2-3 G $\Omega$ , which was consistent with characteristic of second-trimester human neocortical neurons<sup>53</sup>. The input resistances of the NSC-derived neurons on the CNT-multilayered nanomaterials were lower than those on the smooth substrates (Fig. 7I) although not significantly different. Given that neuron electrophysiological maturity is characterized by a relatively hyperpolarized RMP and low input resistances<sup>52,54</sup>, the results in the current study indicated that the CNT-multilayered nanomaterials improved the electrophysiological maturation of the NSC-derived neurons.

More importantly, the electrophysiological neurons derived from the NSCs exhibited clear and fast sodium channel currents, a current component crucial for AP generation<sup>55</sup>, as evidenced from the rapid inward current in response to depolarized membrane potentials (Fig. 7J). Sodium currents and AP spikes disappeared upon treatment with TTX; hence, the currents and spikes in the neurons differentiated from the NSCs were mediated by voltage-gated sodium channels (Fig. 7K). The voltage thresholds for the generation of sodium currents definitely decreased in the sequence of control, PLL, CNT-COOH/PDDA, and CNT@PDA/PDDA although the



differences between these substrates were not significant (Fig. 7L). By contrast, but as expected, the peaks of sodium current significantly increased in the same sequence (Fig. 7M). As the expression of neuronal voltage-gated sodium channels is an essential hallmark of neuronal differentiation toward the mature, electrically active, neuronal phenotype<sup>55-57</sup>, the results in the current study accordingly showed the novel advantages of CNT@PDA/PDDA-multilayered substrates in promoting the functional neuronal maturation of the NSC-derived neurons.

Electrophysiological properties are an important aspect of neuronal maturation in the differentiation phase of early neuronal development<sup>58</sup>. Results herein showed that the CNT@PDA/PDDA-multilayered nanomaterials provided a supporting substrate for promoting the electrophysiological maturity of the NSC-derived neurons in the absence of chemical agents typically required for neurogenesis as evidenced by the capability of firing repetitive APs with various electrophysiological parameters specific to functional and mature neurons, including a RMP close to that of a typical neuron, low membrane resistance, decreased thresholds for the generation of AP and sodium channel current, and increased peaks of AP and sodium channel current. Ballerini *et al.* proposed the “electrotonic hypothesis” that CNTs improve neuronal performance by favoring electrical shortcuts between the proximal and distal compartments of the neuron<sup>59</sup>. Our previous study indicated that CNT nanocomposites fabricated using the LbL assembly of negatively charged CNTs with strong PDDA possessed good conductance<sup>32</sup>.

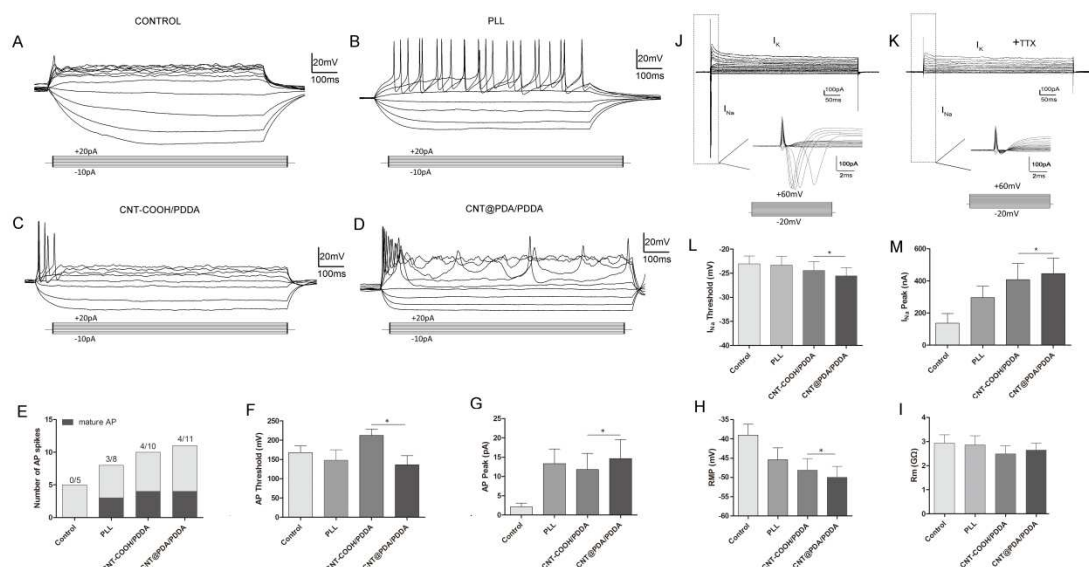


Fig. 7 Electrophysiological properties of NSC-differentiated neurons on different substrates. (A-D) Representative trace of repetitive APs, (E) numbers of mature AP spikes, (F) AP threshold, (G) AP peaks, (H) RMP, (I) input resistances, (J) sodium channel currents, (K) sodium current blocking by TTX, (L) voltage thresholds for the generation of sodium currents, and (M) the peaks of sodium current. (n=60)

## Gene expression profiling investigation on NSC differentiation

The biophysical and biochemical signals in the environment play a critical role in regulating NSC differentiation by inducing the changes in gene expression<sup>17,60,61</sup>. Given that the transcriptome is linked with the genetic information of genome and proteomic biology function, transcriptome sequencing has been increasingly recognized as an efficient means of characterizing the molecular mechanism involved in cell stimulus response<sup>61,62</sup>. In the current study, comprehensive analysis of gene expression profiles after NSC differentiation on various substrates was performed using RNAseq to explore the potential molecular mechanism mediating the observed responses. The expression pattern of DEGs was presented in the heat map of hierarchical clustering in Fig. S1. The expression levels of genes were assigned a color based on the read count in the heat map. When the expression value moved from high to low, the color changed from red to blue. The volcano plots of DEGs in Fig. 8A-8D indicated the degree of DEGs between the CNT-multilayered substrates and the smooth substrates (control and PLL). A high degree of separation represented greater differences of expression between the two groups. As a general observation,

616 NSCs cultured on the CNT-multilayered nanomaterials exhibited profiles with many  
617 DGEs compared with those cultured on the PLL and control substrates. A total of  
618 1531 (1120 up-regulated and 411 down-regulated genes, non-changed 20487 genes)  
619 and 840 (305 up-regulated and 535 down-regulated genes, non-changed 20738 genes)  
620 significant DEGs were identified in the CNT@PDA/PDDA versus PLL and  
621 CNT@PDA/PDDA versus control, respectively. The numbers of DEGs identified in  
622 the CNT-COOH/PDDA versus PLL and CNT-COOH/PDDA versus control were 947  
623 (679 up-regulated and 268 down-regulated genes, non-changed 21072 genes) and 395  
624 (77 up-regulated and 318 down-regulated genes, non-changed 21157 genes),  
625 respectively. Among the significant DEGs versus PLL, CNT@PDA/PDDA and  
626 CNT-COOH/PDDA shared 561 up-regulated and 256 down-regulated genes, whereas  
627 CNT@PDA/PDDA and CNT-COOH/PDDA shared 71 up-regulated and 306  
628 down-regulated genes compared with the control (Fig. 8E). Therefore, CNT@PDA  
629 exerted greater influences on NSCs compared with CNT-COOH as supporting  
630 substrates for NSC growth and differentiation.

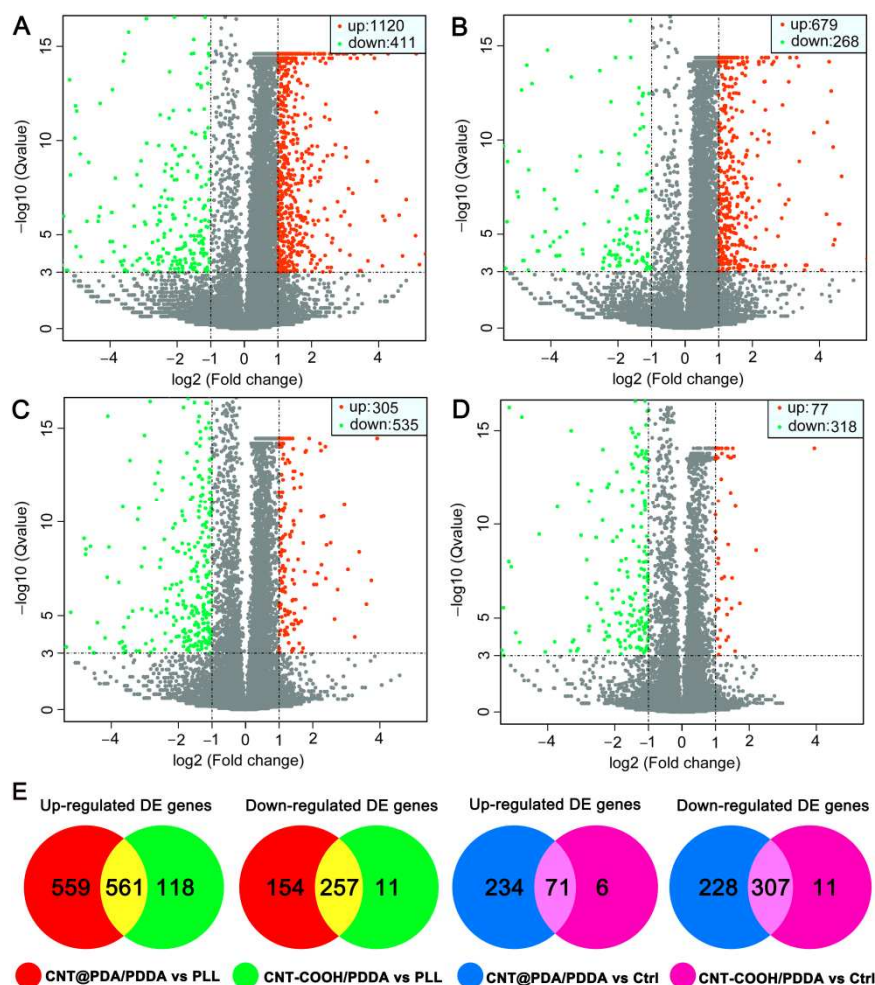


Fig. 8 Volcano plots (A-D) and Venn diagram of DEGs (E). (A) DEGs of NSC on the CNT@PDA/PDDA multilayers versus those on PLL, (B) DEGs of NSC on the CNT-COOH/PDDA multilayers versus those on PLL, (C) DEGs of NSC on CNT@PDA/PDDA multilayers versus those on control, (D) DEGs of NSC on the CNT-COOH/PDDA multilayers versus those on control. (E) The total numbers of up-regulated and down-regulated DEGs in NSCs on the CNT-multilayered substrates as well as the overlaps. (n=3)

GO enrichment analysis, which provided the ontology of defined terms representing gene product properties, was further performed to elucidate the functional properties of genes whose expression significantly changed when NSC differentiation was conducted on CNT multilayers compared with the control and PLL substrates. The threshold for the p-value for multiple testing was set at 0.01, in combination with a threshold of two fold changes in mRNA expression. DEGs were assigned to various functional terms according to the GO database, which were then classified into three categories: biological process (BP), cellular component (CC), and molecular function (MF) (Fig. 9). BP, a recognized series of events or molecular

functions with a defined beginning and end, relevantly reflects the functioning of integrated genes<sup>63</sup>. In comparison with the control substrate, many of the significantly affected GO terms were found to be rooted to various adhesion-associated processes for CNT-multilayered substrates, such as cell adhesions, including cell-substrate adhesion (GO:0031589, 0010810, 0010811, 0010812), cell-matrix adhesion (GO:0007160, 0001953, 0001952), and cell-cell adhesion (GO:0034114, 0034113, 0034116, 0034115); focal adhesion assembly (GO:0048041, 0051894); and cell junctions, including cell-substrate junctions (GO:0090109, 0007044), cell-cell junctions (GO:0045216, 0034329), and adherens junctions (GO:0034333, 0007045, 1903391) (Fig. 8A). CNTs as substrates support cell adhesion, particularly focal adhesion<sup>64,65</sup>, due to the high affinity and thus strong cell-substrate interactions between CNTs and cells<sup>66</sup>. The underlying mechanism, however, has not been well understood until now. In the current study, these significantly involved terms suggested that NSC-derived neural cells intended to form a specialized region of connection between two or more cells or between a cell and the CNT-multilayered substrates. The reorganization of the actin cytoskeleton is a prerequisite for changes in cell shape and motility and gene expression. Therefore, the involved actin-filament-based processes, such as actin-filament-based movement (GO:0030048), regulation of actin-filament-based movement (GO:1903115), and actin-mediated cell contraction (GO:0070252), indicated that the cells anchored on neighboring cells or substrates and moved through the actin filaments. Most of these GO terms were coregulated on the two CNT-multilayered substrates, reflecting the common effects induced by CNTs. However, more significantly regulated genes in every involved GO term on the CNT@PDA multilayers were found than those on the CNT-COOH multilayers (Table S2). Thus, CNT@PDA exerted more extensive regulations to NSC-derived neural cells than CNT-COOH. The regulation on cell adhesion was beneficial to enhance not only cell-substrate interactions but also cell-cell interactions as various biological processes, such as the myelin sheath of axons and formation of BBB in the nervous system, require tight cell-cell interactions. GO terms associated with myelination processes were involved, including axon

678 ensheathment (GO:0008366), neuron ensheathment (GO:0007272), myelination  
 679 (GO:0042552), myelin maintenance (GO:0043217), and axon ensheathment in the  
 680 central nervous system (GO:0032291). The main purpose of a myelin sheath is to  
 681 increase the speed at which impulses propagate along the myelinated axons. Thus, the  
 682 CNT-multilayered substrates, especially the CNT@PDA multilayers, regulated the  
 683 preservation of the structure and function of mature myelin due to the more  
 684 significantly regulated genes than the control substrate.

685 For the CC category, the two CNT-multilayered substrates significantly coregulated  
 686 several GO terms associated with extracellular components, including extracellular  
 687 space (GO:0005615), extracellular matrix (ECM; GO:0031012), proteinaceous ECM  
 688 (GO:0005578), extracellular region part (GO:0044421), extracellular region  
 689 (GO:0005576), collagen trimer (GO:0005581), ECM component (GO:0044420),  
 690 contractile fiber (GO:0043292), fibrillar collagen trimer (GO:0005583), fibrinogen  
 691 complex (GO:0005577), and basement membrane (GO:0005604), compared with the  
 692 control. These significantly regulated CC terms on the CNT-multilayered substrates  
 693 indicated that the CNT multilayers as supporting substrates regulated the secretion of  
 694 ECM components and space structures. Given that ECM is tightly connected to the  
 695 intracellular environment in biology, intracellular signaling, cell-cell adhesion, and  
 696 communication are common functions of the ECM<sup>67</sup>. In this study, GO enrichment  
 697 analyses indicated that gap junction (GO:0005921) belonging to the CC classification  
 698 was also significantly enriched. This finding indicated that the CNT multilayers  
 699 significantly enhanced cell-cell interactions and communication of NSC-derived  
 700 neural cells. Similar to the BP terms, more significantly regulated genes were found in  
 701 every involved CC term on the CNT@PDA multilayers than those on the CNT-COOH  
 702 multilayers. Thus, CNT@PDA exerted more extensive regulations to the  
 703 NSC-derived neural cells than CNT-COOH. Generally, the putative functions of most  
 704 genes are related to binding and transport in the MF category. In the current study, the  
 705 significantly regulated MF-categorized GO terms on the CNT multilayers versus  
 706 control were mainly related to binding activities. The MF classification genes were  
 707 mainly involved in binding-associated terms on the CNT-COOH and CNT@PDA



multilayers, including ECM binding terms, such as ECM structural constituent (GO:0005201), glycosaminoglycan binding (GO:0005539), binding, bridging (GO:0060090), protein binding, and bridging (GO:0030674), and other terms, including heparin binding (GO:0008201), sulfur compound binding (GO:1901681), growth factor binding (GO:0019838), and cell adhesion molecule binding (GO:0050839). The importance of ECM has long been recognized as providing structural and biochemical supports to the surrounding cells. Therefore, these involved GO terms indicated that the CNT-multilayered nanomaterials regulated the selective and noncovalent interactions of the NSC-derived neural cells with ECM components, including structural molecules, growth factors, proteoglycans, and polysaccharides. More terms related to specific binding terms were involved on the CNT@PDA multilayers than on the CNT-COOH multilayers, such as collagen binding (GO:0005518), fibronectin binding (GO:0001968), laminin binding (GO:0043236), and platelet-derived growth factor binding (GO:0048407).

By contrast, the BP-categorized GO terms were mainly related to the metabolic process, catalytic activity, and catabolic process on the CNT-multilayered substrates compared with those on the PLL substrate. This finding indicated that the CNT multilayers exerted significant impacts on the metabolic process of the NSC-derived neural cells (Fig. 8B). The adhesion-related GO terms, however, were seldom observed on the two CNT-multilayered substrates compared with those on the PLL substrate. This finding indicated that the CNT multilayers provided a similar environment for cell adhesion to PLL to a certain extent. Similarly, only few ECM-associated GO terms for the CC category and binding terms for the MF category were identified to be significantly regulated on the two CNT multilayers compared with PLL. These findings indicated that the CNT multilayers provided a permissive environment for neural cell growth.



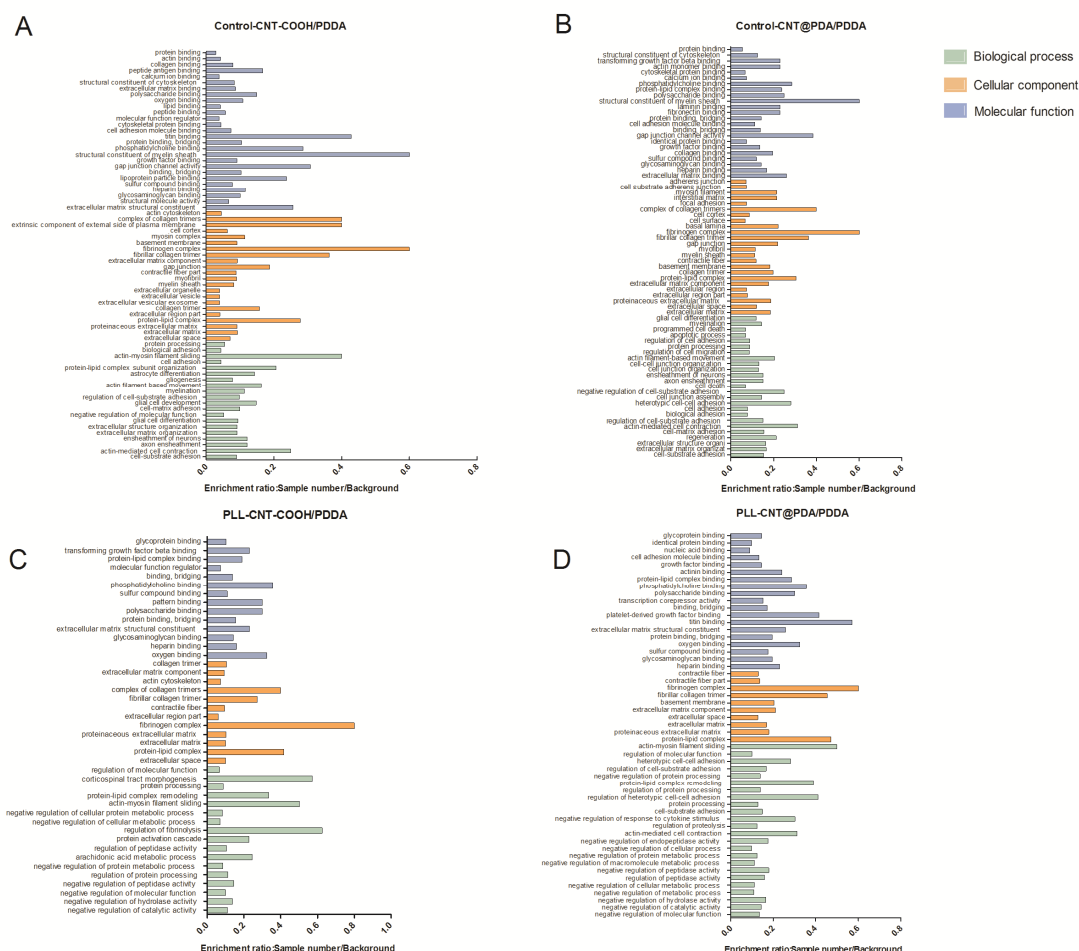


Fig. 9 GO classification of genes on the biological process, cellular component, and molecular function levels on the CNT-COOH/PDDA multilayers versus control (A), CNT@PDA/PDDA multilayers versus control (B), CNT-COOH/PDDA multilayers versus PLL (C), CNT@PDA/PDDA multilayers versus PLL (D). The horizontal axis gives enrichment ratio of sample number/background, while the ordinate gives each detailed classification of GO.

## Signaling pathways

KEGG is a bioinformatics resource for the systematic analysis of gene functions and linking genomic information with higher-order functional information<sup>68</sup>. The pathway-based annotation and analysis can help to further understand high-level biological functions. Therefore, in the current study, these significantly enriched pathways were examined in detail. Similar to the aforementioned GO enrichment analyses, the DEGs identified between the CNT-multilayered substrates (CNT@PDA/PDDA and CNT-COOH/PDDA) and flat substrates (control and PLL) were mapped to the KEGG pathways. The DEGs involved in the cellular processes,

environmental information processing, and organismal systems were focused and further selected based on the following conditions:  $p$ -value  $< 0.05$ , fold change  $> 2$ , and  $\text{RPMK} > 1$  (Fig. 10).

Some cell signaling occurs on a local level when cells interact with the surrounding ECM or with their immediate neighboring cells. This type of signaling plays important roles in tissue and organ morphogenesis and in the maintenance of cell and tissue structure and function. In our study, focal adhesion signaling pathways rooted to cellular processes were significantly involved on the two CNT multilayers in both comparisons with control and PLL. CNTs especially induce focal adhesions at the cell-substrate contact points. Bundles of actin filaments are anchored to transmembrane receptors of integrin through a multimolecular complex of junctional plaque proteins. Focal adhesions form the foci of signal transduction and feedback between the external microenvironment and cells, in which case the signaling mechanisms are crucial in determining cell fate, especially as it relates to differentiation or proliferation<sup>69-72</sup>. Therefore, this study speculated that the CNT multilayers provided a topological substrate with nanoscale features for focal adhesions, some constituents of which were signaling molecules, such as different protein kinases (focal adhesion kinase, FAK) and phosphatases (p-FAK), and various adaptor proteins. These signaling activities initiated downstream signaling events and culminated in the reorganization of the actin cytoskeleton of the NSC-derived neural cells<sup>73</sup>. In addition, negatively charged MWCNTs of nanoscale dimensions adsorb positively charged growth factors secreted by the cells compared with the smooth substrates<sup>17</sup>. Similar morphological alterations and modulation of gene expression are initiated by the binding of growth factors to their respective receptors; hence, considerable crosstalk occurs between adhesion- and growth-factor-mediated signaling. FAK is enriched in developing neuronal bodies and growth cones. This finding suggested that FAK possibly regulates the interactions between the growing neurites and ECM<sup>74</sup>. Reichardt et al. documented that FAK controls axonal dynamics, in part, by regulating the function of Rho family GTPases through the activation of p190RhoGEF. Thus, FAK is an important regulator of axonal development by

controlling the extension and pruning of axon and, consequently, synapse formation<sup>74</sup>. Meanwhile, several signaling pathways involved in environmental information processing were revealed on the CNT multilayers compared with the control. These pathways included the ECM-receptor interaction, PI3K-Akt signaling pathway, FoxO signaling pathway, and cGMP-PKG signaling pathway. These pathways were activated by many types of cellular stimuli and regulate fundamental cellular functions during nervous system development, such as transcription, translation, proliferation, growth, and survival. Specific interactions between cells and the ECM are mediated by transmembrane molecules, mainly integrins, which are a family of transmembrane adhesion receptors consisting of noncovalently bound  $\alpha$ - and  $\beta$ -subunits. Usually, integrins function as mechanoreceptors and mediate cell-substrate signaling by activating intracellular FAK and p-FAK signaling to trigger downstream biochemical signals important for the regulation of gene expression and stem cell fate<sup>75</sup>. CNTs exhibit a strong ability to adsorb proteins through  $\pi$ - $\pi$  interaction<sup>76</sup>. Therefore, the CNT multilayers were assumed to provide a specific environment for ECM-receptor interactions by adsorbing more ECM proteins, e.g., collagen, fibronectin, and laminin, secreted by the NSC-derived cells than the smooth substrates. Interestingly, collagen was the main component of ECM significantly regulated on the CNT-COOH/PDDA multilayers compared with the control and PLL, whereas both collagen and laminin were significantly regulated on the CNT@PDA/PDDA multilayers (Fig. S2). The higher enrichment ratio of KEGG on the CNT@PDA/PDDA multilayers than that on the CNT-COOH/PDDA multilayers agreed with GO analysis presented earlier.

The PI3K-Akt pathway is widely expressed during central nervous system development. It governs embryonic and tissue stem cell self-renewal, maintenance, and regenerative responses<sup>77</sup>. In neurons, the PI3K-Akt pathway can deactivate proapoptotic mediators; activate antiapoptotic proteins; and thus mediate cell survival, differentiation, and metabolism, which participate in neurocyte nutrition and angiogenesis<sup>78</sup>. In addition, accumulating evidences indicated that PI3K-AKT signaling play a neuroprotective role against diverse stresses in the mature CNS, for

example, ethanol-induced neural apoptosis<sup>79</sup> and oxidative stress<sup>80</sup>. In the nervous system, the FoxO signaling pathway is a prominent regulator of adult NSC reserves and lifelong neurogenesis by cell-cycle regulation and oxidative stress suppression<sup>81</sup>. Moreover, FoxO signaling coordinately regulates diverse pathways to govern key aspects of NSC homeostasis. De Pinho et al. demonstrated that FoxO engage the Wnt pathway to ensure a tight regulation of NSCs<sup>82</sup>.

The tight junction signaling pathway was significantly involved on the CNT-COOH/PDDA multilayers compared with the control substrate. As tight junctions are essential for establishing a selectively permeable barrier to diffusion through the paracellular space between neighboring cells, the tight junction signaling pathway plays a pivotal role in regulating cell polarity and hold cells together and is involved in maintaining the blood-brain barrier<sup>83,84</sup>. Recent observations demonstrated that the tight junction signaling pathway is also involved in myelination in nerve systems<sup>83</sup>, through which communications between axon and glial cells are possibly activated and regulated. The VEGF signaling pathway, significantly involved on the CNT@PDA/PDDA multilayers compared with the control and PLL, exhibits a broad range of neurotrophic and neuroprotective effects in the central nervous system by directly stimulating the proliferation of neuronal progenitors. Given the close structural resemblance between the nervous and vascular networks, increasing evidence suggested that VEGF constitutes an important link between neurogenesis and angiogenesis by activating numerous signaling pathways<sup>85</sup>, which in principle improve neurovascular coupling<sup>86</sup>.

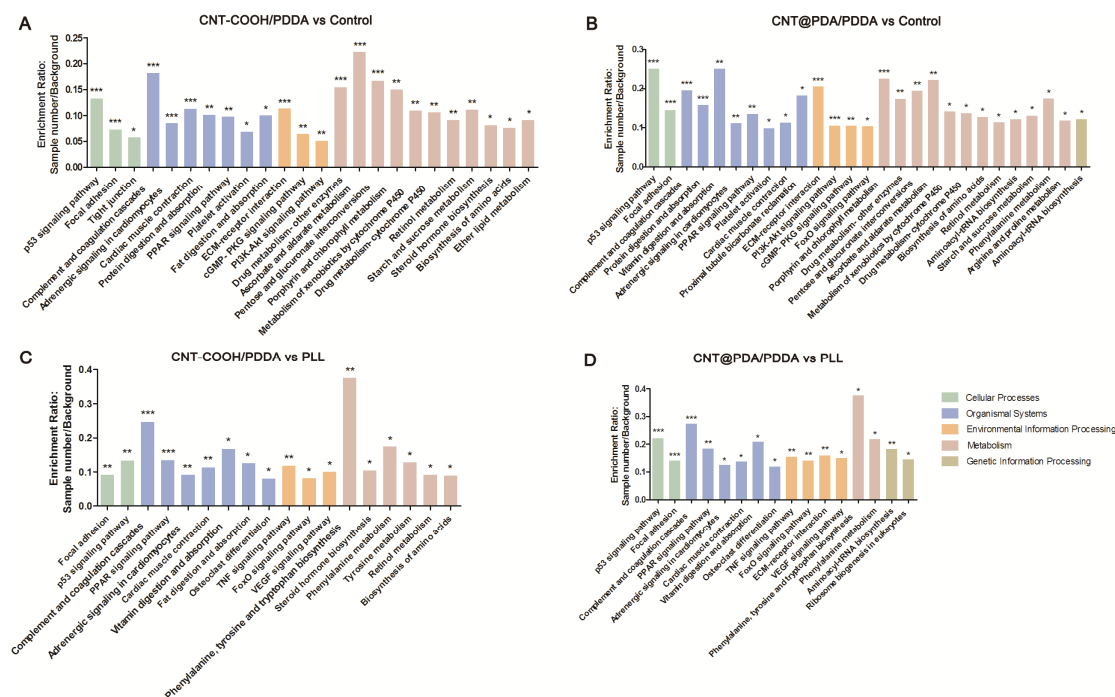


Fig. 10 KEGG enrichment of DGEs on cellular processes, organismal systems, environmental information processing, metabolism, and genetic information processing on the CNT-multilayered substrates versus the smooth substrates. The ordinate gave the KEGG enrichment rate. \*  $p < 0.05$ , \*\*  $p < 0.01$ , \*\*\*  $p < 0.001$ .

During the past decade, CNTs, either used singly or in combination with other biomaterials, have been widely employed in the design of a supporting environment that favor neural functions<sup>87</sup>. Given that CNTs possess a nanostructure similar to neuronal processes (axons and dendrites), numerous studies have documented the unexpected and exciting impacts of CNTs on neuronal signaling. The molecular mechanisms driving these phenomena, however, remain elusive to date. In the current study, CNT multilayers fabricated using the LbL assembly of negatively charged MWCNTs and positively charged PDDA provided a permissive substrate for neuronal differentiation, neurite outgrowth, and electrophysiological maturation of NSC-derived neurons. This study postulated that signal transduction—the process by which physicochemical stimuli of the CNT-multilayered substrate were transmitted through a cell as a series of molecular events—most commonly involved protein phosphorylation catalyzed by protein kinases, which were ultimately integrated into the cellular responses<sup>88-90</sup>. We proposed a possible mechanism of action as illustrated in Fig. 11, the integrin-mediated interactions between the NSCs and CNT multilayers

mainly activated FAK. FAK, a key downstream target, subsequently initiated signaling events, such as the MAPK signaling pathway and Wnt signaling pathway to regulate neural cell proliferation and the PI3K-AKT signaling pathway to regulate neural cell survival. The MAPK signaling pathway regulates neuronal differentiation in NSCs<sup>91,92</sup>. The activated FAK also triggered the Rho family GTPases, which controlled the neurite extension, branching, and consequently synapse formation via the reorganization of the actin cytoskeleton<sup>74,93</sup>. Synaptophysin was formed and was further promoted by tight contact or mechanical strength to increase neuronal electrical signaling capability<sup>17</sup>.

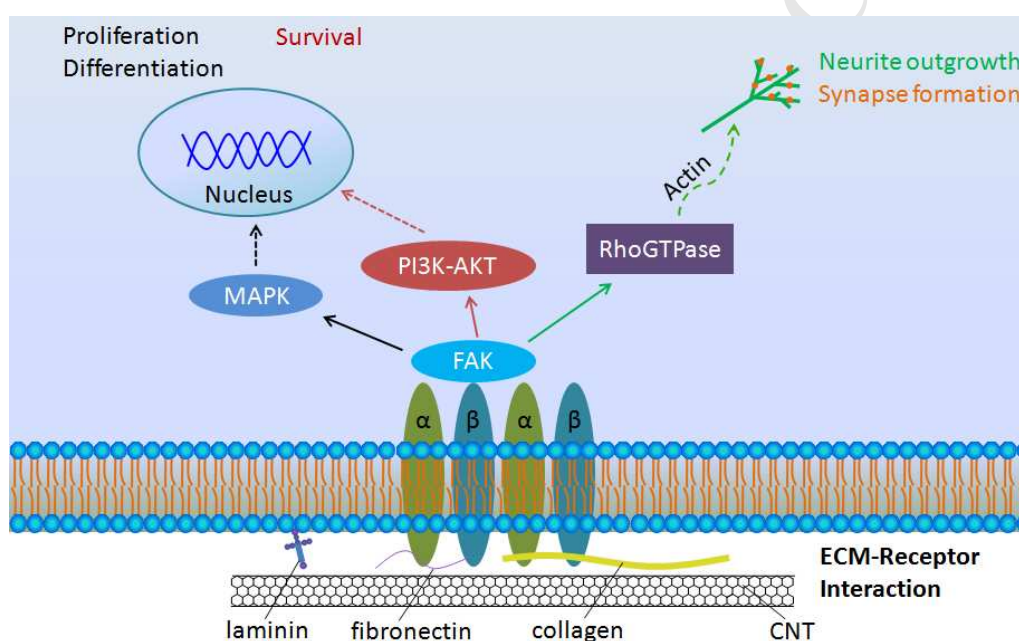


Fig. 11 Schematic diagram of the signal transduction pathways significantly involved in the NSC differentiation on the CNT-multilayered substrates compared with the control and PLL substrates. The ECM proteins (e.g., collagen, fibronectin, and laminin secreted by cells) absorbed on the CNT multilayers interacted with integrin and consequently activated FAK, which subsequently triggered several downstream signaling events to regulate important biological processes, including proliferation, differentiation, survival of NSC, neurite outgrowth, and synapse formation of the NSC-derived neurons.

## Conclusion

In this study, CNT multilayers were prepared using the LbL assembly of negatively charged MWCNTs and positively charged PDDA. The CNT multilayers provided growth substrates with a nanostructure similar to the finest processes of neural cells. Such nanoscaled topographies allowed an unprecedented regulation in the interactions



between neural cells and the nanomaterials themselves, resulting in increased neuronal differentiation, promoted neurite outgrowth, and improved electrophysiological maturation of the NSC-derived neurons. Importantly, the bioinformatics findings indicated that integrins mediated the interactions between NSCs and CNT multilayers and activated endogenous FAK, which subsequently triggered downstream signaling events to regulate neural cell survival, proliferation, differentiation, and synapse formation. As outlined earlier, this study not only presented a construction strategy of CNT-based nanocomposites for neural applications but also facilitated understanding of the mechanism of molecular events involved in the NSC differentiation. With the advancement in nanotechnology and neurobiology, CNT-based nanomaterials would become more relevant in academic research and clinical applications as potent modulators of stem cell behavior.

### Acknowledgements

This work was supported by the National Program on Key Basic Research Project (973 Program, 2014CB542205), the Pearl River Nova Program of Guangzhou (2014J2200001), the Major Science and Technology Projects of Guangdong Province (2015B020225005), the funds of Leading Talents of Guangdong Province (87014002), the Fundamental Research Funds for the Central Universities to Jinan University (11617439), Guangdong special branch plans young talent with scientific and technological innovation (2016TQ03R582) and Guangdong Medical Science and Technology Research Fund Project (A2016387, A010103012).

### References

1. Nho, Y., Kim, J.Y., Khang, D., Webster, T.J. & Lee, J.E. Adsorption of mesenchymal stem cells and cortical neural stem cells on carbon nanotube/polycarbonate urethane. *Nanomedicine (Lond)* **5**, 409-417 (2010).
2. Kumar, S., Rani, R., Dilbaghi, N., Tankeshwar, K. & Kim, K.H. Carbon nanotubes: a novel material for multifaceted applications in human healthcare. *Chemical Society reviews* **46**, 158-196 (2017).
3. John, A.A., *et al.* Carbon nanotubes and graphene as emerging candidates in neuroregeneration and neurodrug delivery. *International journal of nanomedicine* **10**,



- 908 4267-4277 (2015).
- 909 4. Hassanzadeh, P., Arbabi, E., Atyabi, F. & Dinarvand, R. Nerve growth factor-carbon nanotube  
910 complex exerts prolonged protective effects in an in vitro model of ischemic stroke. *Life*  
911 *sciences* **179**, 15-22 (2017).
- 912 5. Yang, Z., et al. Pharmacological and toxicological target organelles and safe use of  
913 single-walled carbon nanotubes as drug carriers in treating Alzheimer disease. *Nanomedicine :  
914 nanotechnology, biology, and medicine* **6**, 427-441 (2010).
- 915 6. Al-Jamal, K.T., et al. Functional motor recovery from brain ischemic insult by carbon  
916 nanotube-mediated siRNA silencing. *Proceedings of the National Academy of Sciences of the*  
917 *United States of America* **108**, 10952-10957 (2011).
- 918 7. Voge, C.M. & Stegemann, J.P. Carbon nanotubes in neural interfacing applications. *Journal of*  
919 *neural engineering* **8**, 011001 (2011).
- 920 8. Keefer, E.W., Botterman, B.R., Romero, M.I., Rossi, A.F. & Gross, G.W. Carbon nanotube  
921 coating improves neuronal recordings. *Nature nanotechnology* **3**, 434-439 (2008).
- 922 9. Jan, E., et al. Layered carbon nanotube-polyelectrolyte electrodes outperform traditional  
923 neural interface materials. *Nano letters* **9**, 4012-4018 (2009).
- 924 10. Landers, J., et al. Carbon nanotube composites as multifunctional substrates for in situ  
925 actuation of differentiation of human neural stem cells. *Advanced healthcare materials* **3**,  
926 1745-1752 (2014).
- 927 11. Yang, D., et al. Graphene oxide promotes the differentiation of mouse embryonic stem cells  
928 to dopamine neurons. *Nanomedicine (Lond)* **9**, 2445-2455 (2014).
- 929 12. Lovat, V., et al. Carbon nanotube substrates boost neuronal electrical signaling. *Nano letters* **5**,  
930 1107-1110 (2005).
- 931 13. Fabbro, A., et al. Spinal cord explants use carbon nanotube interfaces to enhance neurite  
932 outgrowth and to fortify synaptic inputs. *ACS nano* **6**, 2041-2055 (2012).
- 933 14. Lee, J.H., Lee, J.Y., Yang, S.H., Lee, E.J. & Kim, H.W. Carbon nanotube-collagen  
934 three-dimensional culture of mesenchymal stem cells promotes expression of neural  
935 phenotypes and secretion of neurotrophic factors. *Acta biomaterialia* **10**, 4425-4436 (2014).
- 936 15. Bokara, K.K., et al. Biocompatibility of carbon nanotubes with stem cells to treat CNS injuries.  
937 *Anatomy & cell biology* **46**, 85-92 (2013).
- 938 16. Sun, X., et al. Poly(dopamine)-modified carbon nanotube multilayered film and its effects on  
939 macrophages. *Carbon* **113**, 176-191 (2017).
- 940 17. Chen, Y.S. & Hsiue, G.H. Directing neural differentiation of mesenchymal stem cells by  
941 carboxylated multiwalled carbon nanotubes. *Biomaterials* **34**, 4936-4944 (2013).
- 942 18. Jan, E. & Kotov, N.A. Successful differentiation of mouse neural stem cells on layer-by-layer  
943 assembled single-walled carbon nanotube composite. *Nano letters* **7**, 1123-1128 (2007).
- 944 19. Kabiri, M., et al. Neural differentiation of mouse embryonic stem cells on conductive  
945 nanofiber scaffolds. *Biotechnology letters* **34**, 1357-1365 (2012).
- 946 20. Jin, G.Z., Kim, M., Shin, U.S. & Kim, H.W. Neurite outgrowth of dorsal root ganglia neurons is  
947 enhanced on aligned nanofibrous biopolymer scaffold with carbon nanotube coating.  
948 *Neuroscience letters* **501**, 10-14 (2011).
- 949 21. GhoshMitra, S., Diercks, D.R., Mills, N.C., Hynds, D.L. & Ghosh, S. Role of engineered  
950 nanocarriers for axon regeneration and guidance: current status and future trends. *Advanced*  
951 *drug delivery reviews* **64**, 110-125 (2012).

- 952 22. Kim, Y.G., *et al.* Differential stimulation of neurotrophin release by the biocompatible  
953 nano-material (carbon nanotube) in primary cultured neurons. *Journal of biomaterials*  
954 *applications* **28**, 790-797 (2014).
- 955 23. Hu, H., Ni, Y., Montana, V., Haddon, R.C. & Parpura, V. Chemically Functionalized Carbon  
956 Nanotubes as Substrates for Neuronal Growth. *Nano letters* **4**, 507-511 (2004).
- 957 24. Fabbro, A., Bosi, S., Ballerini, L. & Prato, M. Carbon nanotubes: artificial nanomaterials to  
958 engineer single neurons and neuronal networks. *ACS chemical neuroscience* **3**, 611-618  
959 (2012).
- 960 25. Cellot, G., *et al.* Carbon nanotube scaffolds tune synaptic strength in cultured neural circuits:  
961 novel frontiers in nanomaterial-tissue interactions. *The Journal of neuroscience : the official*  
962 *journal of the Society for Neuroscience* **31**, 12945-12953 (2011).
- 963 26. Mehra, N.K., Mishra, V. & Jain, N.K. A review of ligand tethered surface engineered carbon  
964 nanotubes. *Biomaterials* **35**, 1267-1283 (2014).
- 965 27. Zykowska, A., Radji-Taleb, S. & Cuenot, S. Layer-by-layer functionalization of carbon  
966 nanotubes with synthetic and natural polyelectrolytes. *Langmuir : the ACS journal of surfaces*  
967 *and colloids* **26**, 2779-2784 (2010).
- 968 28. Dieckmann, G.R., *et al.* Controlled assembly of carbon nanotubes by designed amphiphilic  
969 Peptide helices. *Journal of the American Chemical Society* **125**, 1770-1777 (2003).
- 970 29. Gopalakrishnan, R., Balamurugan, K., Singam, E.R., Sundaraman, S. & Subramanian, V.  
971 Adsorption of collagen onto single walled carbon nanotubes: a molecular dynamics  
972 investigation. *Physical chemistry chemical physics : PCCP* **13**, 13046-13057 (2011).
- 973 30. Zheng, M., *et al.* DNA-assisted dispersion and separation of carbon nanotubes. *Nature*  
974 *materials* **2**, 338-342 (2003).
- 975 31. Paloniemi, H., *et al.* Water-soluble full-length single-wall carbon nanotube polyelectrolytes:  
976 preparation and characterization. *The journal of physical chemistry. B* **109**, 8634-8642 (2005).
- 977 32. Shao, H., *et al.* Fabrication of carbon nanotube nanocomposites via layer-by-layer assembly  
978 and evaluation in biomedical application. *Nanomedicine (Lond)* **11**, 3087-3101 (2016).
- 979 33. Mamedov, A.A., *et al.* Molecular design of strong single-wall carbon  
980 nanotube/polyelectrolyte multilayer composites. *Nature materials* **1**, 190-194 (2002).
- 981 34. Audic, S. & Claverie, J.M. The significance of digital gene expression profiles. *Genome*  
982 *research* **7**, 986-995 (1997).
- 983 35. Fraczek-Szczypta, A. Carbon nanomaterials for nerve tissue stimulation and regeneration.  
984 *Materials science & engineering. C, Materials for biological applications* **34**, 35-49 (2014).
- 985 36. Liu, Y., Ai, K. & Lu, L. Polydopamine and its derivative materials: synthesis and promising  
986 applications in energy, environmental, and biomedical fields. *Chemical reviews* **114**,  
987 5057-5115 (2014).
- 988 37. Gottipati, M.K., Kalinina, I., Bekyarova, E., Haddon, R.C. & Parpura, V. Chemically  
989 functionalized water-soluble single-walled carbon nanotubes modulate morpho-functional  
990 characteristics of astrocytes. *Nano letters* **12**, 4742-4747 (2012).
- 991 38. Defterali, C., *et al.* In Vitro Evaluation of Biocompatibility of Uncoated Thermally Reduced  
992 Graphene and Carbon Nanotube-Loaded PVDF Membranes with Adult Neural Stem  
993 Cell-Derived Neurons and Glia. *Frontiers in bioengineering and biotechnology* **4**, 94 (2016).
- 994 39. Worle-Knirsch, J.M., Pulskamp, K. & Krug, H.F. Oops they did it again! Carbon nanotubes hoax  
995 scientists in viability assays. *Nano letters* **6**, 1261-1268 (2006).

- 996 40. Zhao, P., *et al.* Cytotoxic and adhesion-associated response of NIH-3T3 fibroblasts to  
997 COOH-functionalized multi-walled carbon nanotubes. *Biomed Mater* **11**, 015021 (2016).
- 998 41. Huang, Y.J., Wu, H.C., Tai, N.H. & Wang, T.W. Carbon nanotube rope with electrical stimulation  
999 promotes the differentiation and maturity of neural stem cells. *Small* **8**, 2869-2877 (2012).
- 1000 42. Lustgarten, J.H., *et al.* Semipermeable polymer tubes provide a microenvironment for in vivo  
1001 analysis of dorsal root regeneration. *Journal of biomechanical engineering* **113**, 184-188  
1002 (1991).
- 1003 43. Mattson, M.P., Haddon, R.C. & Rao, A.M. Molecular functionalization of carbon nanotubes  
1004 and use as substrates for neuronal growth. *Journal of molecular neuroscience : MN* **14**,  
1005 175-182 (2000).
- 1006 44. Fernandes, A., *et al.* Bilirubin as a determinant for altered neurogenesis, neuritogenesis, and  
1007 synaptogenesis. *Developmental neurobiology* **69**, 568-582 (2009).
- 1008 45. Meiri, K.F. & Gordon-Weeks, P.R. GAP-43 in growth cones is associated with areas of  
1009 membrane that are tightly bound to substrate and is a component of a membrane skeleton  
1010 subcellular fraction. *The Journal of neuroscience : the official journal of the Society for*  
1011 *Neuroscience* **10**, 256-266 (1990).
- 1012 46. Mongiu, A.K., Weitzke, E.L., Chaga, O.Y. & Borisy, G.G. Kinetic-structural analysis of neuronal  
1013 growth cone veil motility. *Journal of cell science* **120**, 1113-1125 (2007).
- 1014 47. Biggs, M.J., Richards, R.G. & Dalby, M.J. Nanotopographical modification: a regulator of  
1015 cellular function through focal adhesions. *Nanomedicine : nanotechnology, biology, and*  
1016 *medicine* **6**, 619-633 (2010).
- 1017 48. Gabay, T., Jakobs, E., Ben-Jacob, E. & Hanein, Y. Engineered self-organization of neural  
1018 networks using carbon nanotube clusters. *Physica A* **350**, 611-621 (2005).
- 1019 49. Gabay, T., *et al.* Electro-chemical and biological properties of carbon nanotube based  
1020 multi-electrode arrays. *Nanotechnology* **18**, 035201 (2007).
- 1021 50. Sorkin, R., *et al.* Process entanglement as a neuronal anchorage mechanism to rough surfaces.  
1022 *Nanotechnology* **20**, 015101 (2009).
- 1023 51. Mazzatenta, A., *et al.* Interfacing neurons with carbon nanotubes: electrical signal transfer  
1024 and synaptic stimulation in cultured brain circuits. *The Journal of neuroscience : the official*  
1025 *journal of the Society for Neuroscience* **27**, 6931-6936 (2007).
- 1026 52. Gunhanlar, N., *et al.* A simplified protocol for differentiation of electrophysiologically mature  
1027 neuronal networks from human induced pluripotent stem cells. *Molecular psychiatry* (2017).
- 1028 53. Moore, A.R., *et al.* Electrical excitability of early neurons in the human cerebral cortex during  
1029 the second trimester of gestation. *Cerebral cortex* **19**, 1795-1805 (2009).
- 1030 54. Kemp, P.J., *et al.* Improving and accelerating the differentiation and functional maturation of  
1031 human stem cell-derived neurons: role of extracellular calcium and GABA. *The Journal of*  
1032 *physiology* **594**, 6583-6594 (2016).
- 1033 55. Fabbro, A., *et al.* Adhesion to carbon nanotube conductive scaffolds forces action-potential  
1034 appearance in immature rat spinal neurons. *PloS one* **8**, e73621 (2013).
- 1035 56. Biella, G., *et al.* Differentiating embryonic stem-derived neural stem cells show a  
1036 maturation-dependent pattern of voltage-gated sodium current expression and graded action  
1037 potentials. *Neuroscience* **149**, 38-52 (2007).
- 1038 57. Wang, K., *et al.* Critical roles of voltage-dependent sodium channels in the process of  
1039 synaptogenesis during the postnatal cortical development of rats. *Cellular and molecular*

- 1040 *neurobiology* **29**, 1131-1142 (2009).
- 1041 58. Spitzer, N.C. Electrical activity in early neuronal development. *Nature* **444**, 707-712 (2006).
- 1042 59. Cellot, G., *et al.* Carbon nanotubes might improve neuronal performance by favouring  
1043 electrical shortcuts. *Nature nanotechnology* **4**, 126-133 (2009).
- 1044 60. Mercado, A.T., *et al.* The effect of chemically modified electrospun silica nanofiber on the  
1045 mRNA and miRNA expression profile of neural stem cell differentiation. *Journal of biomedical*  
1046 *materials research. Part A* **104**, 2730-2743 (2016).
- 1047 61. Xia, B., Zou, Y., Xu, Z. & Lv, Y. Gene expression profiling analysis of the effects of low-intensity  
1048 pulsed ultrasound on induced pluripotent stem cell-derived neural crest stem cells.  
1049 *Biotechnology and applied biochemistry* **64**, 927-937 (2017).
- 1050 62. Tang, C., Lan, D., Zhang, H., Ma, J. & Yue, H. Transcriptome analysis of duck liver and  
1051 identification of differentially expressed transcripts in response to duck hepatitis A virus  
1052 genotype C infection. *PloS one* **8**, e71051 (2013).
- 1053 63. Li, S.C., *et al.* Assessment of nanomaterial cytotoxicity with SOLiD sequencing-based  
1054 microRNA expression profiling. *Biomaterials* **32**, 9021-9030 (2011).
- 1055 64. Patel, K.D., *et al.* Nanostructured biointerfacing of metals with carbon nanotube/chitosan  
1056 hybrids by electrodeposition for cell stimulation and therapeutics delivery. *ACS applied*  
1057 *materials & interfaces* **6**, 20214-20224 (2014).
- 1058 65. Ryoo, S.R., Kim, Y.K., Kim, M.H. & Min, D.H. Behaviors of NIH-3T3 fibroblasts on  
1059 graphene/carbon nanotubes: proliferation, focal adhesion, and gene transfection studies. *ACS*  
1060 *nano* **4**, 6587-6598 (2010).
- 1061 66. Kato, M. & Mrksich, M. Using model substrates to study the dependence of focal adhesion  
1062 formation on the affinity of integrin-ligand complexes. *Biochemistry* **43**, 2699-2707 (2004).
- 1063 67. Abedin, M. & King, N. Diverse evolutionary paths to cell adhesion. *Trends in cell biology* **20**,  
1064 734-742 (2010).
- 1065 68. Kanehisa, M. & Goto, S. KEGG: kyoto encyclopedia of genes and genomes. *Nucleic acids*  
1066 *research* **28**, 27-30 (2000).
- 1067 69. Dong, Y., Sun, H., Li, X., Li, X. & Zhao, L. Impact of Carbon Nanomaterials on Actin  
1068 Polymerization. *Journal of nanoscience and nanotechnology* **16**, 2408-2417 (2016).
- 1069 70. Huber, F., *et al.* Emergent complexity of the cytoskeleton: from single filaments to tissue.  
1070 *Advances in physics* **62**, 1-112 (2013).
- 1071 71. Pollard, T.D. & Borisy, G.G. Cellular motility driven by assembly and disassembly of actin  
1072 filaments. *Cell* **112**, 453-465 (2003).
- 1073 72. Mahmood, T.A., de Jong, R., Riesle, J., Langer, R. & van Blitterswijk, C.A. Adhesion-mediated  
1074 signal transduction in human articular chondrocytes: the influence of biomaterial chemistry  
1075 and tenascin-C. *Experimental cell research* **301**, 179-188 (2004).
- 1076 73. Keselowsky, B.G., Collard, D.M. & Garcia, A.J. Surface chemistry modulates focal adhesion  
1077 composition and signaling through changes in integrin binding. *Biomaterials* **25**, 5947-5954  
1078 (2004).
- 1079 74. Rico, B., *et al.* Control of axonal branching and synapse formation by focal adhesion kinase.  
1080 *Nature neuroscience* **7**, 1059-1069 (2004).
- 1081 75. Chen, W., *et al.* Nanotopography influences adhesion, spreading, and self-renewal of human  
1082 embryonic stem cells. *ACS nano* **6**, 4094-4103 (2012).
- 1083 76. Ge, C., *et al.* Binding of blood proteins to carbon nanotubes reduces cytotoxicity. *Proceedings*

- of the National Academy of Sciences of the United States of America **108**, 16968-16973 (2011).
77. Paling, N.R., Wheadon, H., Bone, H.K. & Welham, M.J. Regulation of embryonic stem cell self-renewal by phosphoinositide 3-kinase-dependent signaling. *The Journal of biological chemistry* **279**, 48063-48070 (2004).
78. Arboleda, G., Morales, L.C., Benitez, B. & Arboleda, H. Regulation of ceramide-induced neuronal death: cell metabolism meets neurodegeneration. *Brain research reviews* **59**, 333-346 (2009).
79. Tapodi, A., *et al.* Pivotal role of Akt activation in mitochondrial protection and cell survival by poly(ADP-ribose)polymerase-1 inhibition in oxidative stress. *The Journal of biological chemistry* **280**, 35767-35775 (2005).
80. de la Monte, S.M., *et al.* Partial rescue of ethanol-induced neuronal apoptosis by growth factor activation of phosphoinositide-3-kinase. *Alcoholism, clinical and experimental research* **24**, 716-726 (2000).
81. Hu, F., Xu, P., Sun, B., Teng, G. & Xiao, Z. Deep sequencing reveals complex mechanisms of microRNA regulation during retinoic acid-induced neuronal differentiation of mesenchymal stem cells. *Genomics* **109**, 302-311 (2017).
82. Paik, J.H., *et al.* FoxOs cooperatively regulate diverse pathways governing neural stem cell homeostasis. *Cell stem cell* **5**, 540-553 (2009).
83. Gonzalez-Mariscal, L., Betanzos, A., Nava, P. & Jaramillo, B.E. Tight junction proteins. *Progress in biophysics and molecular biology* **81**, 1-44 (2003).
84. Wacker, B.K., Freie, A.B., Perfater, J.L. & Gidday, J.M. Junctional protein regulation by sphingosine kinase 2 contributes to blood-brain barrier protection in hypoxic preconditioning-induced cerebral ischemic tolerance. *Journal of cerebral blood flow and metabolism : official journal of the International Society of Cerebral Blood Flow and Metabolism* **32**, 1014-1023 (2012).
85. Kowanetz, M. & Ferrara, N. Vascular endothelial growth factor signaling pathways: therapeutic perspective. *Clinical cancer research : an official journal of the American Association for Cancer Research* **12**, 5018-5022 (2006).
86. Ahmad, S., *et al.* Direct evidence for endothelial vascular endothelial growth factor receptor-1 function in nitric oxide-mediated angiogenesis. *Circulation research* **99**, 715-722 (2006).
87. Fabbro, A., Prato, M. & Ballerini, L. Carbon nanotubes in neuroregeneration and repair. *Advanced drug delivery reviews* **65**, 2034-2044 (2013).
88. Vogel, V. & Sheetz, M. Local force and geometry sensing regulate cell functions. *Nature reviews. Molecular cell biology* **7**, 265-275 (2006).
89. Zhao, C., Tan, A., Pastorin, G. & Ho, H.K. Nanomaterial scaffolds for stem cell proliferation and differentiation in tissue engineering. *Biotechnology advances* **31**, 654-668 (2013).
90. Huang, H., Kamm, R.D. & Lee, R.T. Cell mechanics and mechanotransduction: pathways, probes, and physiology. *American journal of physiology. Cell physiology* **287**, C1-11 (2004).
91. Sweatt, J.D. The neuronal MAP kinase cascade: a biochemical signal integration system subserving synaptic plasticity and memory. *Journal of neurochemistry* **76**, 1-10 (2001).
92. Fukunaga, K. & Miyamoto, E. Role of MAP kinase in neurons. *Molecular neurobiology* **16**, 79-95 (1998).

- 1128 93. Navarro, A.I. & Rico, B. Focal adhesion kinase function in neuronal development. *Current*  
1129 *opinion in neurobiology* **27**, 89-95 (2014).